Resource

Cell Chemical Biology

An RNA-Based Fluorescent Biosensor for High-Throughput Analysis of the cGAS-cGAMP-STING Pathway

Graphical Abstract

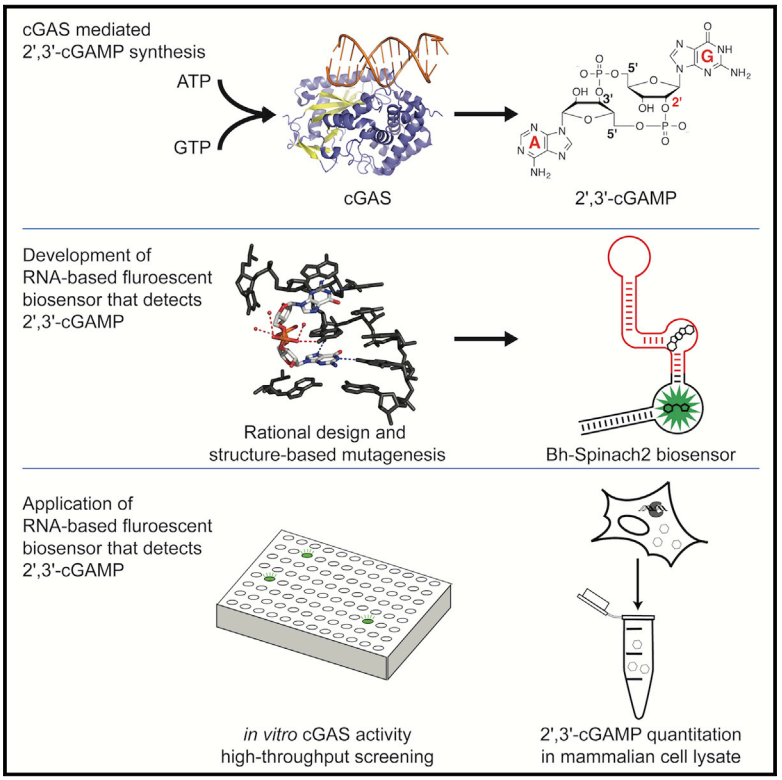

Highlights

- A fluorescent biosensor that responds to 2′,3′-cGAMP was designed
- A biosensor-based fluorescence turn-on assay detects cGAS activity and inhibition
- High-throughput analysis via fluorescence plate reader is enabled
- 2′,3′-cGAMP levels were quantified in DNA-stimulated L929 cells

Authors

Debojit Bose, Yichi Su, Assaf Marcus, David H. Raulet, Ming C. Hammond

Correspondence

mingch@berkeley.edu

In Brief

Bose et al. developed a fluorescent biosensor for the mammalian immune signal 2′,3′-cGAMP that enables high-throughput screening assays and quantitation of cGAS enzyme activity. Biosensor-based assays revealed that DNA intercalators indirectly modulate cGAS activity and quantitated the amount of 2′,3′-cGAMP produced in DNA-stimulated L929 cells.

Bose et al., 2016, Cell Chemical Biology *23*, 1–11
December 22, 2016
http://dx.doi.org/10.1016/j.chembiol.2016.10.014

CellPress

Please cite this article in press as: Bose et al., An RNA-Based Fluorescent Biosensor for High-Throughput Analysis of the cGAS-cGAMP-STING Pathway, Cell Chemical Biology (2016), http://dx.doi.org/10.1016/j.chembiol.2016.10.014

Cell Chemical Biology
Resource

An RNA-Based Fluorescent Biosensor for High-Throughput Analysis of the cGAS-cGAMP-STING Pathway

Debojit Bose,[1,3] Yichi Su,[1,3] Assaf Marcus,[2] David H. Raulet,[2] and Ming C. Hammond[1,2,4,*]
[1]Department of Chemistry
[2]Department of Molecular & Cell Biology
University of California, Berkeley, CA 94720, USA
[3]Co-first author
[4]Lead Contact
*Correspondence: mingch@berkeley.edu
http://dx.doi.org/10.1016/j.chembiol.2016.10.014

SUMMARY

In mammalian cells, the second messenger (2′–5′,3′–5′) cyclic guanosine monophosphate-adenosine monophosphate (2′,3′-cGAMP), is produced by the cytosolic DNA sensor cGAMP synthase (cGAS), and subsequently bound by the stimulator of interferon genes (STING) to trigger interferon response. Thus, the cGAS-cGAMP-STING pathway plays a critical role in pathogen detection, as well as pathophysiological conditions including cancer and autoimmune disorders. However, studying and targeting this immune signaling pathway has been challenging due to the absence of tools for high-throughput analysis. We have engineered an RNA-based fluorescent biosensor that responds to 2′,3′-cGAMP. The resulting "mix-and-go" cGAS activity assay shows excellent statistical reliability as a high-throughput screening (HTS) assay and distinguishes between direct and indirect cGAS inhibitors. Furthermore, the biosensor enables quantitation of 2′,3′-cGAMP in mammalian cell lysates. We envision this biosensor-based assay as a resource to study the cGAS-cGAMP-STING pathway in the context of infectious diseases, cancer immunotherapy, and autoimmune diseases.

INTRODUCTION

The mammalian innate immune system uses pattern recognition receptors (PRRs) to sense extracellular or intracellular pathogens by recognizing pathogen-associated molecular patterns to trigger the proper immune response. Nucleic acid sensors are one important class of PRRs that recognize foreign DNA or RNA upon microbial infection and other pathophysiological conditions. The cGAS/stimulator of interferon genes (STING) pathway was recently discovered to be an important cytosolic immune surveillance pathway (Ishikawa and Barber, 2008; Sun et al., 2013). cGAS is a universal DNA sensor that is activated upon binding to cytosolic DNA to produce the signaling molecule (2′–5′,3′–5′) cyclic guanosine monophosphate (GMP)-AMP (Ablasser et al., 2013; Diner et al., 2013; Gao et al., 2013b). Acting as a second messenger during microbial infection, 2′,3′-cGAMP binds and activates STING, leading to production of type I interferon (IFN) and other co-stimulatory molecules that trigger the immune response (Ahn et al., 2014; Gao et al., 2013a; Hansen et al., 2014; Watson et al., 2015). STING also has been shown to recognize bacterial-derived cyclic dinucleotides and elicit the type I IFN response (Barker et al., 2013; Burdette et al., 2011). Natural variants in human STING have differential specificity in recognizing cyclic dinucleotides. While human R232 STING protein (and the mouse R231 counterpart) can be stimulated by 2′,3′-cGAMP, bacterial 3′,3′-cGAMP and bacterial c-di-GMP (Gao et al., 2013a), human H232 STING is only responsive to 2′,3′-cGAMP (Diner et al., 2013; Gao et al., 2013a; Zhang et al., 2013).

Besides its role in infectious disease, the cGAS/STING pathway has emerged as a promising new target for cancer immunotherapy and autoimmune diseases (Ahn et al., 2015; Baird et al., 2016; Corrales and Gajewski, 2015; Corrales et al., 2015; Curran et al., 2015; Demaria et al., 2015; Deng et al., 2014; Woo et al., 2014, 2015b). DNA fragments present in the tumor microenvironment are proposed to activate cGAS in dendritic cells (DC), followed by IFN-induced DC maturation and activation of a potent and beneficial immune response against cancer cells (Woo et al., 2015a). In a separate context, dysregulation of the cGAS/STING pathway has been implicated in self-DNA-triggered inflammatory and autoimmune disorders, such as systemic lupus erythematosus and Aicardi-Goutieres syndrome (Ahn et al., 2012, 2014; Gao et al., 2015).

With increasing evidence that the cGAS/STING pathway is involved in immune responses to microbial pathogens and cancer cells, and may play a role in autoimmune disorders, it is critical to explore its regulation and activation status. However, deconvoluting the role of the cGAS/STING pathway in immune responses is made difficult by the presence of multiple surveillance pathways that trigger the same IFN signal downstream. For example, one of the most commonly used and sensitive methods to detect activation of the cGAS/STING pathway is a luciferase reporter fused to an IFN-β promoter (Diner et al., 2013). However, other DNA sensors (e.g., TLR9), RNA sensors

(e.g., RIG, MDA5), and immune modulators also activate expression of this reporter as all of them activate downstream IFN production (Shrivastav and Niewold, 2013). In addition, the assay requires transfection of the reporter DNA, and this foreign DNA can activate cGAS and other DNA-sensing pathways, which can mask the underlying physiology. Thus, it would be advantageous to have a direct method of detecting and quantifying 2′,3′-cGAMP rather than downstream signals, for diagnostic purposes and for clearly distinguishing cGAS/STING from other nucleic acid-sensing pathways, to determine its contribution to the overall immune response and expand our understanding of its regulation.

Furthermore, a detection method for 2′,3′-cGAMP that is adaptable to a high-throughput screening (HTS) format is desirable for biomedical applications, as efforts are underway to develop small-molecule modulators of the cGAS/STING pathway for cancer immunotherapy and vaccine development. While current efforts have focused on targeting STING with natural and unnatural cyclic dinucleotides and the small-molecule DMXAA (Baird et al., 2016; Chandra et al., 2014; Corrales et al., 2015; Demaria et al., 2015; Deng et al., 2014; Downey et al., 2014; Kobayashi et al., 2015; Nakamura et al., 2015; Zhang et al., 2015), cGAS may be an advantageous drug target because activating the enzyme can produce an amplified signal relative to the STING receptor small-molecule interaction. cGAS also may be an attractive target for small-molecule inhibition in the case of autoimmune diseases.

Unfortunately, current in vitro methods to detect 2′,3′-cGAMP have specific limitations to their utility. Thin-layer chromatography (TLC) assays utilizing radioactive nucleotide substrates to detect 2′,3′-cGAMP produced by cGAS in vitro cannot be used to quantify endogenous 2′,3′-cGAMP levels inside the cell or in cell lysates. Liquid chromatography-mass spectrometry (LC-MS) has been used to detect cyclic dinucleotides in bacterial cell extracts (Burhenne and Kaever, 2013; Waters, 2010) and mammalian cell extracts (Wu et al., 2013). Importantly, however, neither of these methods is readily adapted to HTS formats nor offers the potential for live cell imaging.

Both fundamental and applied studies of the cGAS/STING immune signaling pathway would greatly benefit from a direct and high-throughput method to assay cGAS activity. However, the natural protein receptor for 2′,3′-cGAMP, STING, is poorly suited for engineering a fluorescent biosensor, because it functions as a homodimer and its structure precludes facile connection of the protein chains or circular permutation. Overexpression of STING-based constructs in vivo also may activate downstream responses, which would be an undesired physiological effect. To our knowledge, no other receptors for 2′,3′-cGAMP have been reported.

Here we describe the development of fluorescent biosensors that exhibit a turn-on response to 2′,3′-cGAMP. We designed the biosensors by making rational mutations to natural riboswitch aptamers of the GEMM-II class that recognize the related molecule 3′,3′-cyclic di-GMP (c-di-GMP) (Lee et al., 2010). Using one of these 2′,3′-cGAMP biosensors, we showed direct detection of cGAS enzymatic activity by a fluorescence readout in a 384-well format, by fluorescence-based detection of overexpressed cGAS activity in bacterial lysates by a plate reader and in live bacteria by flow cytometry, and by fluorescence-based quantitation of endogenous cGAS activity in DNA-stimulated lysates from the L929 mammalian cell line. Our in vitro enzymatic assays showed that nucleic acid intercalators can indirectly inhibit cGAS activity. Finally, analysis of mammalian cell lysates revealed that 60 attomoles, or 36 million molecules, of 2′,3′-cGAMP are produced on average per cell upon DNA stimulation in the L929 cell line.

RESULTS

Engineering a Fluorescent Biosensor to Sense 2′,3′-cGAMP

Previously, our laboratory developed RNA-based fluorescent biosensors selective for c-di-GMP or 3′,3′-cGAMP based on natural GEMM-I riboswitches (Kellenberger et al., 2013, 2015). However, these biosensors did not respond at all to 2′,3′-cGAMP, even though some of the parent riboswitch aptamers exhibited very high specificity and affinity to 3′,3′-cGAMP (Kellenberger et al., 2015; Ren et al., 2015). X-ray crystal structures of ligand-bound GEMM-I riboswitches showed extensive interactions with the 2′-hydroxyls and phosphodiester oxygens of c-di-GMP or 3′,3′-cGAMP (Figures S1A and S1B) (Ren et al., 2015; Shanahan et al., 2011; Smith et al., 2011). These interactions would be disrupted by the 2′–5′ linkage present in 2′,3′-cGAMP.

We instead reasoned that the GEMM-II riboswitch scaffold may be more amenable for engineering a 2′,3′-cGAMP biosensor (Figure 1A). The canonical ligand for this riboswitch class is c-di-GMP; however, X-ray crystal structures showed that there are few canonical Watson-Crick or Hoogsteen pairing interactions between ligand nucleobases and the riboswitch, and few hydrogen bonds between the ligand backbone and the riboswitch (Figures S1A and S1B). This suggests that GEMM-II may have some flexibility in base recognition. Furthermore, the GEMM-II riboswitch aptamer from *Clostridium acetobutylicum* has been reported to accept c-di-GMP analogs with modifications to the ribose and phosphates (Shanahan et al., 2011; Smith et al., 2011), which was promising for tolerating changes to the backbone linkage.

Four characterized GEMM-II riboswitches (Lee et al., 2010; Smith et al., 2011) were picked to design 16 biosensor candidates with varied-length transducer stems derived from the natural riboswitch P1 stems (Table S1). These biosensors were initially screened for fluorescence turn-on and binding affinity to c-di-GMP, the canonical ligand (Figure S1C), then the four most-promising biosensors were further profiled for response to c-di-GMP, 3′,3′-cGAMP, and 2′,3′-cGAMP (Figure S1D). One of the candidates that incorporated a GEMM-II riboswitch from *Bacillus halodurans C-125*, Bh P1-5 delC, exhibited a fluorescence response to micromolar concentrations of 2′,3′-cGAMP. The name indicates that the riboswitch portion of the biosensor is fused to the Spinach2 aptamer via a five-base-paired P1 stem with deletion of a single C present in the natural stem bulge (Figure 1A).

While Bh P1-5 delC showed good affinity for 2′,3′-cGAMP (apparent dissociation constant, K_D = 13.4 ± 0.9 μM) at 37°C, 3 mM Mg^{2+} (Figure 1B), the related Bh P1-6 showed lower background fluorescence and higher activation (5-fold) with c-di-GMP (Figures S1C and S1D), which allowed us to analyze the

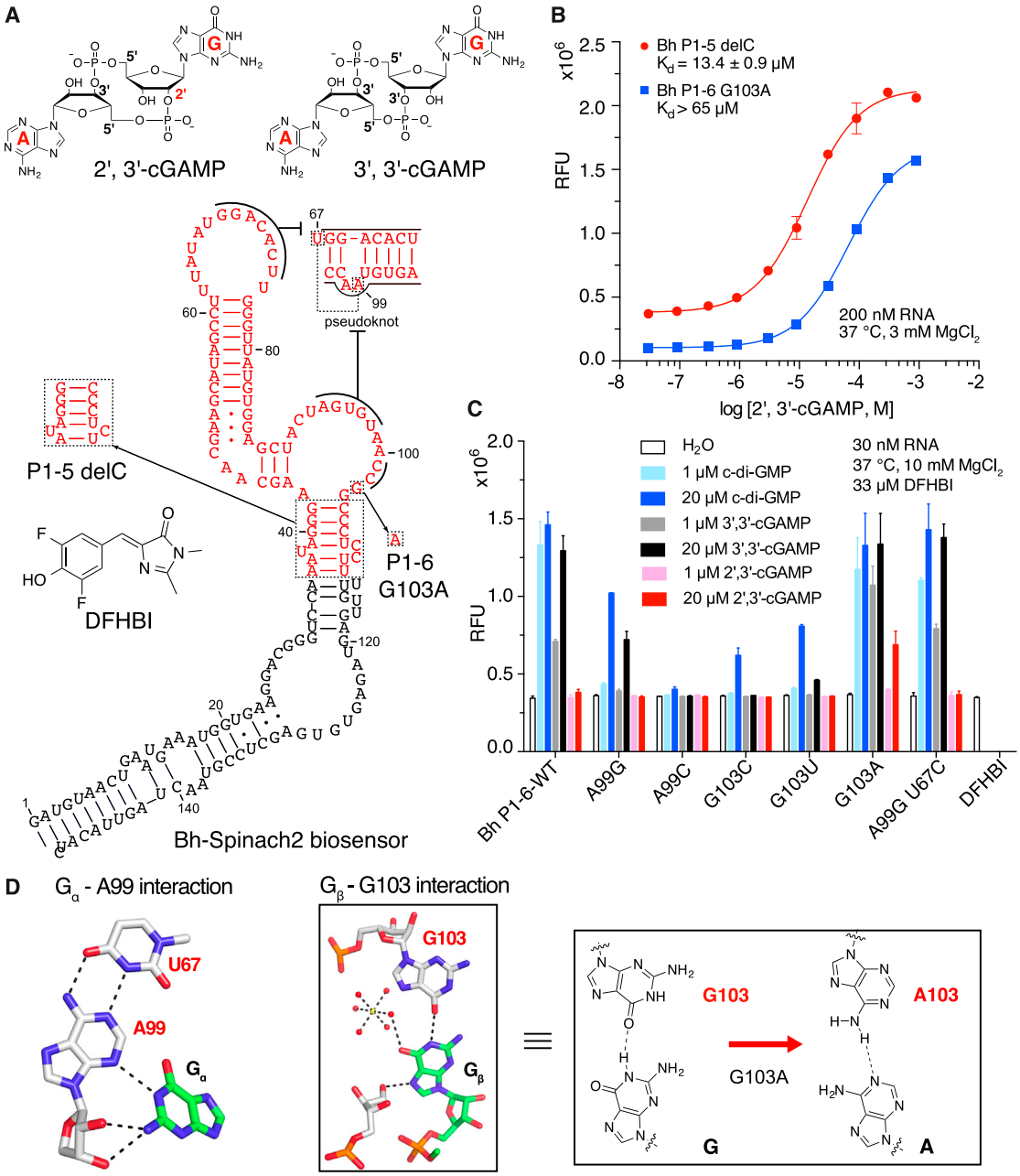

Figure 1. Development of RNA-Based Fluorescent Biosensors for 2′,3′-cGAMP

(A) Chemical structures of 3′,3′-cGAMP, 2′,3′-cGAMP, and DFHBI. Secondary structure model of GEMM-II riboswitch-based biosensors that detect 2′,3′-cGAMP. Key mutations that led to first-generation biosensors are boxed and labeled.

(B) In vitro fluorescence activation and binding-affinity measurements for RNA-based biosensors with 2′,3′-cGAMP.

(C) Analysis of the effect of binding pocket mutations on biosensor response to different cyclic dinucleotides.

(D) Hydrogen bonding interactions between the GEMM-II riboswitch and G_α and G_β of c-di-GMP (PDB: 3Q3Z) and the proposed effect of the G103A mutation on recognition of the adenine in 2′,3′-cGAMP. Error bars represent SD for three independent replicates. RFU, relative fluorescence units.

effect of mutations on ligand selectivity. Two positions in the riboswitch binding pocket that make direct contacts with the ligand nucleobases were mutagenized and the fluorescence response to 2′,3′-cGAMP was examined (Figures 1C and 1D). Whereas mutations to A99, the position that recognizes G_α of c-di-GMP, did not improve the response to 2′,3′-cGAMP, we observed fluorescence activation by 2′,3′-cGAMP with G103A, which mutates the position that recognizes G_β of c-di-GMP.

The effect of the G103A mutation can be rationalized as establishing a hydrogen bond with the A base of 3′,3′-cGAMP or 2′,3′-cGAMP, and disfavoring interaction with the G base of c-di-GMP. Accordingly, we found that the cyclic dinucleotide

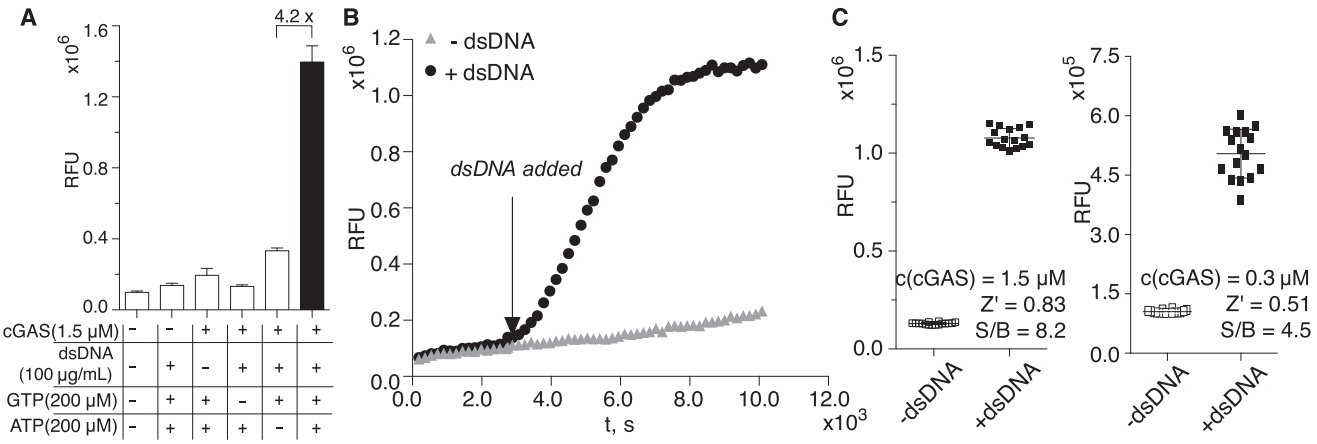

Figure 2. Application of Fluorescent Biosensor to cGAS Enzyme Activity Assays

(A) Bh P1-6 G103A biosensor detects 2′,3′-cGAMP produced in the cGAS enzyme reaction (black). Enzyme reactions that lack one component served as negative controls (white).

(B) In situ detection of cGAS activity by the RNA-based fluorescent biosensor.

(C) Determination of the Z′ factors for cGAS activity assay using the RNA-based biosensor in a 384-well format. Error bars represent SD for 3 (A) or 16 (C) independent replicates.

selectivity profile for the Bh P1-6 G103A biosensor was switched relative to wild-type Bh P1-6 (Table S2). The binding affinity to 3′,3′-cGAMP was increased by more than 10-fold (K_D from >11 to 0.8 μM), whereas the binding affinity to c-di-GMP was reduced by more than 125-fold (K_D from 56 nM to >7 μM). Furthermore, improved binding extended to 2′,3′-cGAMP, such that 200 nM Bh P1-6 G103A showed 5-fold fluorescence activation in response to 20 μM ligand, whereas the wild-type biosensor had shown no response (Figures 1B and S1).

We had expected that the same G103A mutation could be applied to the Bh P1-5 delC biosensor but, disappointingly, it resulted in complete loss of biosensor function (Figure S1E). High fluorescence was observed even in the absence of the ligand, which implies that this single-nucleotide substitution, in conjunction with deleting one nucleotide in the stem bulge, favors formation of a stable transducer stem in the absence of the ligand. Nevertheless, by combining rational design and structure-based mutagenesis, we have developed two fluorescent biosensors capable of detecting 2′,3′-cGAMP at micromolar concentrations. A detailed comparison of their binding affinities and fluorescent turn-on properties is given in Table S2. Similar to STING, the native protein receptor for 2′,3′-cGAMP, the biosensors also respond to the bacterial second messengers c-di-GMP and 3′,3′-cGAMP, but otherwise exhibit high selectivity against other metabolites such as ATP and GTP (Figure 2A). Importantly, whereas STING is a homodimeric protein that is not readily adaptable as a fluorescent biosensor, we have generated a first-generation fluorescent biosensor for 2′,3′-cGAMP based on the GEMM-II riboswitch scaffold.

Assaying cGAS Activity In Vitro Using a Fluorescent Biosensor

Currently, the established method to assay cGAS activity in vitro is via TLC analysis of radiolabeled nucleotides (Figure S2A) (Diner et al., 2013). Although it is accurate and highly sensitive, this method uses radioactive materials, which poses increased safety concerns and hampers adaptation as a HTS assay. These issues could be overcome by using fluorescent biosensors to assay cGAS enzyme activity.

We analyzed the enzymatic activity of the DNA sensor cGAS using the Bh P1-6 G103A biosensor, which has lower background fluorescence and higher turn-on. Upon binding to DNA, cGAS is activated to catalyze the 2′–5′ phosphodiester bond formation between GTP and ATP, followed by cyclization to form the 3′–5′ bond (Ablasser et al., 2013). As expected, the biosensor gives a strong fluorescence signal only when all components of the reaction are present to enable robust production of 2′,3′-cGAMP (Figure 2A). Besides carrying out assays in a standard mix-and-go format, in which the enzyme reactions are performed separately from the biosensor detection reactions, we also showed that the biosensor can be employed for direct in situ detection, e.g., the biosensor functions in the enzymatic reaction buffer (Figure 2B).

Minor fluorescence increases were also detected in control reactions without DNA or without ATP. The former was due to incomplete removal of DNA during purification of cGAS enzyme, resulting in the observed basal activation. The latter could be caused by the formation of either pppGp(2′–5′)G or 2′,3′-c-di-GMP, which have been previously reported as minor products in the absence of ATP (Ablasser et al., 2013). We did not test biosensor response to these side products because of the difficulty in obtaining sufficient amounts for binding measurements; however, the signal-to-background ratio is still quite good even when comparing the enzyme reactions with and without ATP (4.2×).

Due to the involvement of the cGAS/STING pathway in multiple pathophysiological conditions, a high-throughput screen for its modulators is highly desirable. Since the biosensor-based fluorescent assay can be performed in a 384-well plate and analyzed in a fluorescent plate reader, it is readily adapted to HTS for activators or inhibitors of cGAS. With a 1.5 μM concentration of cGAS, we determined a Z′ factor of 0.83 and a

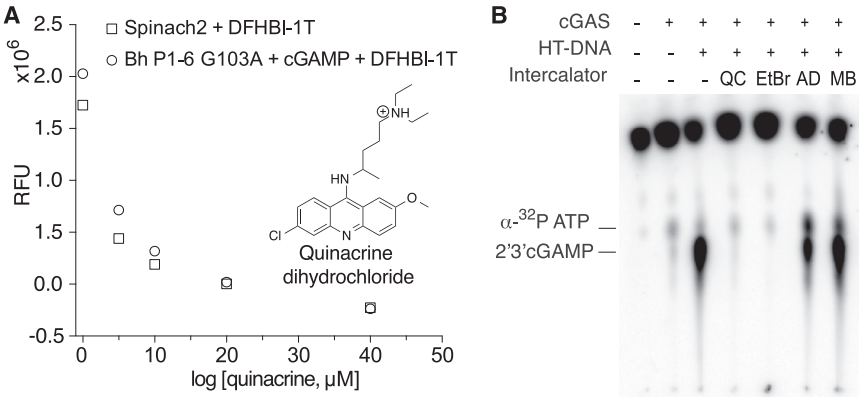

Figure 3. The Effect of Nucleic Acid Intercalators on the Fluorescence of RNA-Based Biosensors and cGAS Activity

(A) Observation of dose-dependent loss of fluorescence in the presence of quinacrine for both the 2′,3′-cGAMP biosensor and the Spinach2 aptamer. (B) TLC-based activity assay to assess cGAS inhibition by quinacrine (QC), ethidium bromide (EtBr), actinomycin D (AD), and methylene blue (MB).

signal-to-background ratio of 8.2× for the assay in this format, where a Z′ factor >0.5 is considered to be an assay with excellent statistical reliability for HTS (Figure 2C) (Zhang et al., 1999). To screen for high-affinity inhibitor or activator compounds, the assay would need to be performed with nanomolar concentrations of enzyme. We obtained a Z′ factor of 0.51 and a signal-to-background ratio of 4.5× using the RNA biosensor, 300 nM enzyme, and manual pipetting of all reagents in 384-well format (Figure 2C). Thus, we expect that the current fluorescent biosensor enables HTS assays for moderate affinity (e.g., 300–500 nM dissociation constant) compounds that affect cGAS activity.

Revealing a Limitation of the Biosensor Assay and an Alternative Mechanism of Small-Molecule Inhibition of cGAS

Quinacrine, a well-characterized anti-malarial drug, has been reported to inhibit cGAS activity, with a half maximal inhibitory concentration IC_{50} value of 13 μM measured by the radiolabeled TLC assay (An et al., 2015). We attempted to demonstrate inhibitor characterization using our fluorescent biosensor assay (Figure S2B), but a control experiment revealed that the decrease in fluorescence signal was independent of enzyme activity (Figure 3A). Quinacrine is a known DNA intercalator (Boer et al., 2009) and we reasoned that it may disrupt biosensor function by intercalating into the RNA helices (Sinha et al., 2007). This appeared to be the case, as we showed that quinacrine also decreased fluorescence of the dye-binding Spinach2 aptamer (Figure 3A). This observation reveals an inherent limitation of RNA-based biosensors, which is that intercalating compounds may yield false-positive fluorescent changes. However, RNA-based biosensors have been successfully used to characterize inhibitors that specifically target proteins, including methyltransferases (Su et al., 2016) and RNA demethylases (Svensen and Jaffrey, 2016).

By the same logic, we realized that quinacrine likely inhibits cGAS activity indirectly by interfering with DNA binding. Previous studies inferred that quinacrine intercalation would lengthen the B-form DNA helix based on circular dichroism measurements, but otherwise would not grossly alter conformation (Hossain et al., 2008). To support our hypothesis about mechanism of action, we tested other DNA intercalators for effects on cGAS activity. The radiolabeled TLC assay was employed to avoid possible complications in data interpretation from compounds interacting with the RNA biosensor. Quinacrine and ethidium bromide have similar DNA binding modes (LePecq and Paoletti, 1967), and both fully inhibited cGAS activity at 100 μM concentration. Actinomycin D, which binds to single-stranded and double-stranded DNA, showed partial inhibition at that concentration, whereas methylene blue, which intercalates in a completely different orientation than quinacrine (Hossain et al., 2008), had no effect (Figure 3B). These results provide strong evidence that nucleic acid intercalators are a class of small-molecule compounds capable of inhibiting cGAS. Our results and those from the original study with quinacrine (An et al., 2015) do not distinguish whether inhibition is via a direct or indirect mechanism, but we favor the latter, e.g., that these compounds intercalate and shift the DNA helix conformation sufficiently to reduce binding to cGAS enzyme. We can easily analyze the enzyme-independent effect of compounds on fluorescence of the RNA-based biosensors in control reactions, which allows us to identify compounds in the screen that likely interact with the DNA instead of the enzyme directly, a potential source for false-positive hits. Overall, our analysis of the limitation of the capacity of our RNA-based biosensor to characterize cGAS inhibition by intercalating compounds led to an important finding on alternate mechanisms of cGAS inhibition by small molecules, and revealed the advantage of using the RNA biosensor to distinguish nucleic acid intercalators from direct cGAS inhibitors.

Quantitating 2′,3′-cGAMP in Lysates of DNA-Stimulated Mammalian Cells

A critical aim is to detect cGAS activation in mammalian cells. Based on our positive results in detecting cGAS overexpression in bacteria (Figure S3), we considered applying the fluorescent biosensor to detect cellular cGAMP levels in mammalian cell lysates. 2′,3′-cGAMP is produced by cGAS+ mammalian cells as part of a cytosolic immune surveillance pathway for foreign DNA, which could be caused by viral or bacterial infection and, alternatively, by leakage of damaged nuclear or mtDNA (Gao et al., 2013a; Hansen et al., 2014; Li et al., 2016; Ma and Damania, 2016; Watson et al., 2015; White et al., 2014; Woo et al., 2015a). A standard method to simulate these conditions is to transfect cells with double-stranded DNA; however, it has not been straightforward to directly measure the levels of 2′,3′-cGAMP produced. Besides MS, which is a low-throughput method, the main method to study this pathway involves an IFN-β reporter assay, which is highly sensitive but has drawbacks in that it requires prior transfection of the reporter DNA and is not specific to the cGAS-STING pathway, other immune

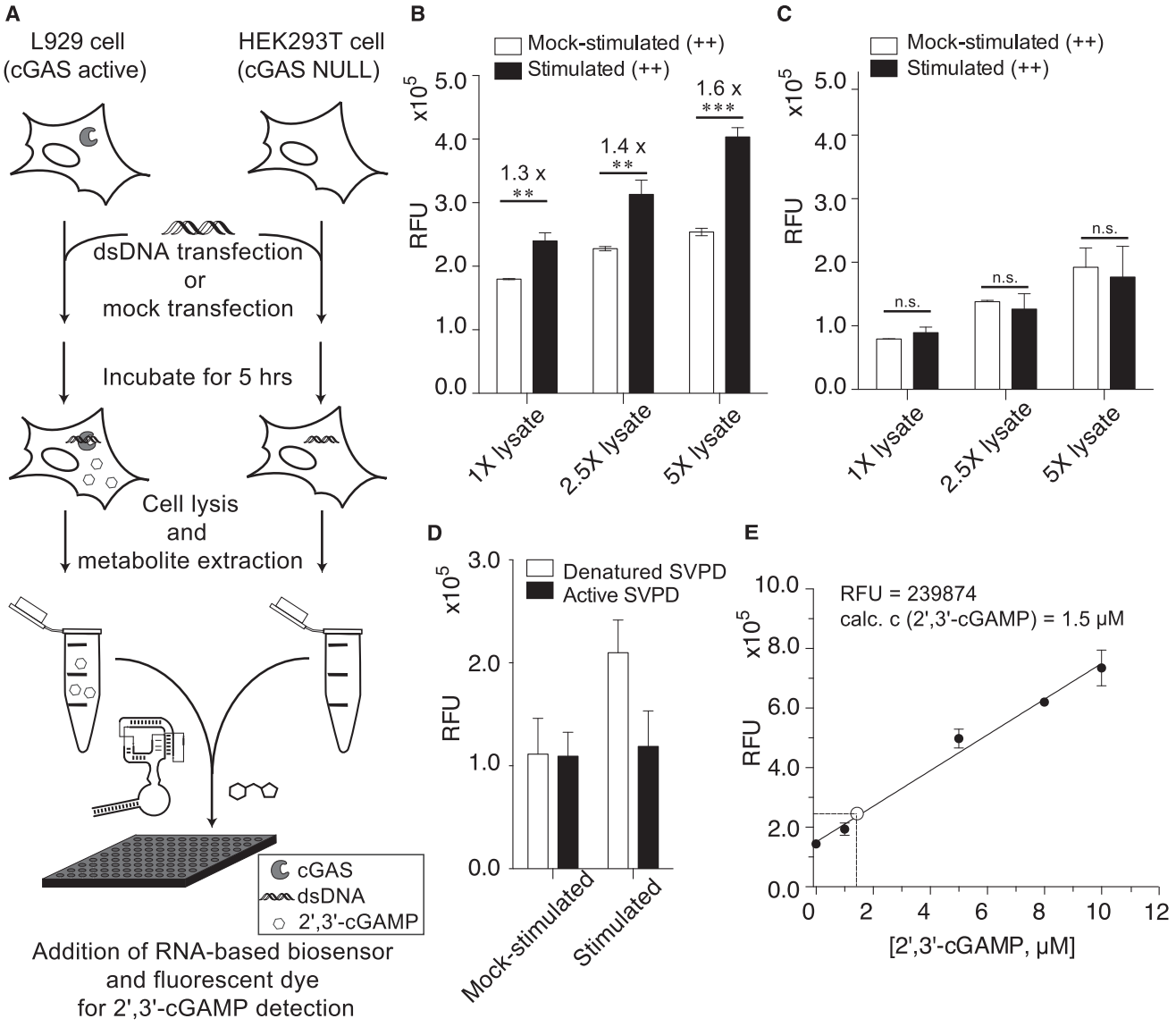

Figure 4. Application of the Fluorescent Biosensor to Detect 2′,3′-cGAMP in Mammalian Cell Extracts

(A) Schematic representation of the experimental procedure for cell extract analysis using the fluorescent biosensor.

(B and C) Fluorescence readings for different concentrations of L929 (B) or HEK293T (C) cell extracts (DNA- or mock-stimulated).

(D) Fluorescence readings for L929 cell extracts (DNA- or mock-stimulated) treated with active or denatured SVPD prior to biosensor addition.

(E) Standard curve of fluorescence readings from mock-stimulated L929 cell extracts doped with known concentrations of 2′,3′-cGAMP (black circles). Average fluorescence readings from DNA-stimulated L929 cell extracts shown as open circles.

Error bars represent the SD for three (B and C) or two (D and E) independent biological replicates. p Values are calculated from Student's t test comparison: **$p < 0.01$, ***$p < 0.001$, n.s., not significant, $p > 0.05$.

signaling also stimulates IFN production and activates the promoter controlling reporter expression.

We evaluated the ability of the fluorescent biosensor to detect 2′,3′-cGAMP produced upon DNA stimulation of cGAS+ L929 cells (Sun et al., 2013). In comparison, we also analyzed mock-transfected L929 cells that express functional cGAS, and HEK293T cells that are cGAS null under identical conditions. In vitro measurements were performed by adding aliquots of cell lysate to the fluorescent biosensor reaction in a 96-well plate reader (Figure 4A). Fluorescence activation was observed for DNA-stimulated over mock-stimulated L929 cells, with an increasing turn-on signal upon addition of 1–5 µL of concentrated cell lysate (3×10^5 cells per µL of concentrated cell extract) (Figure 4B). In contrast, no significant fluorescence change between DNA-stimulated and mock-stimulated cells was observed for HEK293T cells (Figure 4C). Thus, we showed that our first-generation biosensor has sufficient sensitivity to detect endogenous 2′,3′-cGAMP produced in response to DNA activation of the cGAS enzyme in human cell lysates.

Interestingly, we observed a higher background fluorescence signal for mock-stimulated L929 cells than for HEK293T cells. We checked whether there was basal 2′,3′-cGAMP in mock-stimulated L929 cells that were activating the fluorescent biosensor. Background fluorescence for the mock-stimulated sample did not change upon treatment with active snake venom phosphodiesterase (SVPD), which degrades 2′,3′-cGAMP (Diner et al., 2013) (Figures 4D and S4). In contrast, active SVPD did reduce the fluorescence signal of DNA-stimulated L929 cell lysates to the same levels as mock-stimulated samples. Therefore, we concluded that the observed difference in background fluorescence was due to distinct levels of auto-fluorescence between the cell types and includes contributions to background fluorescence from the presence of the dye DFHBI and the RNA biosensor (Figure S4).

Finally, using our fluorescent biosensor we were able to determine the absolute concentration of 2′,3′-cGAMP produced upon DNA stimulation in L929 cells. Mock-stimulated L929 cell lysate was doped with known concentrations of 2′,3′-cGAMP and the corresponding biosensor fluorescence signals were measured to obtain a standard curve with a lower limit of detection of 0.95 μM (Figure 4E). The fluorescence signal from L929 cells stimulated with DNA for 5 hr was compared with the standard curve, and showed that there was a concentration of 1.5 μM for 2′,3′-cGAMP in L929 cell lysate. Assuming 100% extraction efficiency, it was calculated that DNA stimulation by transfection resulted in 60 attomoles of 2′,3′-cGAMP produced on average per L929 cell, or 36 million molecules of 2′,3′-cGAMP per cell (Figure 4E, see Supplemental Experimental Procedures for detailed calculations).

DISCUSSION

Even though no natural riboswitches for 2′,3′-cGAMP have been discovered, we were able to engineer RNA-based fluorescent biosensors for 2′,3′-cGAMP by employing structure-based rational design. Ligand-bound riboswitch structures informed the initial choice of the GEMM-II scaffold and mutations to the ligand binding pocket. A modest screen of different phylogenetic and stem variants was guided by empirical design rules for functional biosensors that start with use of the natural P1 stem (Kellenberger and Hammond, 2015; Wang et al., 2016). Our results in this study again demonstrate that riboswitch-based biosensors can be reprogrammed to recognize other ligands via point mutations, although not necessarily with full selectivity (Kellenberger et al., 2013; Ren et al., 2015; Wu et al., 2015). The broader implication is that natural riboswitch-ligand pairs can serve as advanced starting points for the engineering of biosensors for related ligands not recognized by known riboswitches. In one case, this actually led to the rational discovery of natural riboswitches (Kellenberger et al., 2015).

Our biosensors exhibit fluorescence turn-on activity in direct response to 2′,3′-cGAMP and thus are readily adapted for HTS assays of cGAS enzyme activity and inhibition. Given the emerging clinical relevance of the cGAS/STING innate immune signaling pathway for infectious diseases, cancer immunotherapy, and DNA-triggered autoimmune disorders, a fluorescent plate reader screen for small-molecule modulators of cGAS activity is a timely and valuable resource for the academic and industrial research community. We evaluated the Z′ factor for the assay, which showed that high signal-to-background ratios gave statistically reliable results. The ability to use DFHBI analogs with different fluorescent emission wavelengths (Song et al., 2014) may be further beneficial to avoid false-positive hits. We also showed that our assay provides a straightforward way to distinguish between compounds that target cGAS enzyme versus those that interact with the activating ligand, double-stranded DNA.

Our finding that intercalating compounds affect cGAS activation reveals that the mechanism of small-molecule inhibition of cGAS enzyme should be carefully examined. In addition, since DNA intercalators are used as anti-cancer drugs (Wheate et al., 2007), it potentially raises interesting questions about the activation status of cGAS during drug treatment. There also are broader implications for the design of synthetically modified double-stranded nucleic acids for therapeutic or basic research purposes. In particular, we expect that backbone modifications that favor B-form-like helical conformations may cause the nucleic acid agent to bind and activate cGAS, thus triggering the IFN response. This adds to the existing body of knowledge about the length and sequence requirements for cGAS activation (Gao et al., 2013b; Herzner et al., 2015; Li et al., 2013), and further implies that some synthetic modifications may be better at eluding cGAS surveillance and thus the cytosolic immune response. Our assay provides a rapid, non-radioactive, and low material cost method to screen nucleic acid agents for such activity.

Finally, we have employed a fluorescent biosensor to quantitate the levels of 2′,3′-cGAMP in L929 cell lysates, which previously had been shown to be cGAS+ via LC-MS analysis (Sun et al., 2013), but not in a quantitative manner. Very recently, an LC-MS/MS method has been developed for quantitation of 2′,3′-cGAMP (Paijo et al., 2016). The amount of 2′,3′-cGAMP produced upon human cytomegalovirus infection was measured in the range of 0.1–0.3 attomoles, or 60,000–180,000 molecules, on average per cell, depending on the cell type (Paijo et al., 2016). As expected, we have found that transfection of DNA leads to a much stronger response, as we measured 60 attomoles of 2′,3′-cGAMP on average per cell at an earlier time point (6 hr post-transfection versus 24 hr post-infection). Based on the standard curve in L929 lysates, the current lower limit of detection of our fluorescent biosensor is ~1 μM or 40 attomoles per cell. Thus, improving biosensor sensitivity by 133- to 400-fold would provide a high-throughput method to analyze viral-induced 2′,3′-cGAMP levels in the future. Perhaps more excitingly, this analysis suggests that second-generation fluorescent biosensors with the requisite higher sensitivity, e.g., binding affinities in the 2.5–7.5 nM range, would be useful for single-cell analysis of 2′,3′-cGAMP production upon virus infection. In addition, biosensors with improved sensitivity would enable high-throughput biochemical and/or cell-based assays for high-affinity compounds that modulate cGAS activity. We recently described a phylogenetic search strategy for generating high-affinity and high turn-on RNA-based biosensors, which resulted in a biosensor capable of detecting subnanomolar levels of cyclic di-GMP (Wang et al., 2016). Work on applying this methodology to the 2′,3′-cGAMP sensor is ongoing in the laboratory.

Much in the way that antibody-based assays are indispensable for analysis of kinase signaling, fluorescent biosensor-based

assays will be a valuable resource for the analysis of cyclic dinucleotide signaling. Measuring 2′,3′-cGAMP levels is important for investigating the basic biology of the cGAS-STING signaling pathway and its mechanistic contribution to innate immune responses. A recent study showed that, in a viral infection model, cGAS and STING expression levels do not necessarily correlate with 2′,3′-cGAMP production, and furthermore that 2′,3′-cGAMP levels do not necessarily correlate with IFN production (Paijo et al., 2016). These findings underscore the importance of measuring cGAS enzyme activity, rather than using its expression level or induction of IFN as proxies. In the context of cancer immunology, it has been suggested that tumor-derived DNA activates cGAS activity in host immune cells (Woo et al., 2015b), but direct proof of this hypothesis is still lacking. Addressing these and other pressing questions about cGAS activity will be facilitated by a high-throughput fluorescent plate reader assay capable of quantitating 2′,3′-cGAMP levels directly from lysates of different mammalian cell types. We also demonstrate use of the biosensor for both biochemical and cell-based analysis of cGAS activity, which provides two different HTS methods to identify chemical compounds or novel protein factors that affect cGAS activity.

SIGNIFICANCE

To our knowledge, this study demonstrates the first fluorescent plate reader assay for detection of 2′,3′-cGAMP, a signaling molecule central to the cGAS/STING innate immune pathway that has emerged as a promising new target for cancer immunotherapy and therapy of autoimmune diseases. The assay relies on a riboswitch-based fluorescent biosensor that was generated by structure-based rational design. Several intercalating compounds were found to affect cGAS activity, which has broader implications for related anti-cancer agents and the design of synthetically modified double-stranded nucleic acids for therapeutic or basic research purposes. Finally, as proof of principle, we demonstrated quantitation of 2′,3′-cGAMP from DNA-stimulated cell lysates using the fluorescent biosensor.

EXPERIMENTAL PROCEDURES

Reagents and Oligonucleotides

DNA oligonucleotides for biosensor constructs were purchased as Ultramers from Integrated DNA Technologies and other DNA oligonucleotides were purchased from Elim Biopharmaceuticals. DFHBI and DFHBI-1T were either purchased from Lucerna or were synthesized following previously described protocols (Song et al., 2014) and were stored as 10–30 mM stocks in DMSO. c-di-GMP, 3′,3′-cGAMP, 2′,3′-cGAMP were purchased from Axxora. Commercially available reagents were used without further purification. T7 RNA polymerase was either purchased from New England Biolabs or given as a generous gift by the laboratory of Terrence Oas at Duke University. Phusion DNA polymerase was purchased from New England Biolabs. Chemically competent BL21 (DE3) Star cells were purchased from Life Technologies. Quinacrine dihydrochloride, herring testes DNA (HT-DNA), and SVPD was purchased from Sigma-Aldrich. L929 and HEK293T cells were purchased from ATCC.

In Vitro Transcription

DNA templates for in vitro transcription were prepared through PCR amplification using Phusion DNA polymerase (New England Biolabs) from sequence-confirmed plasmids using primers that added the T7 polymerase promoter sequence. PCR products were purified by a QIAquick PCR purification kit (QIAGEN) for characterization and application experiments. Templates were then transcribed using T7 RNA polymerase in 40 mM Tris-HCl (pH 8.0), 6 mM $MgCl_2$, 2 mM spermidine, and 10 mM DTT. RNAs were either purified by a 96-well format ZR-96 Clean & Concentrator (Zymo Research) for the candidate biosensor screen or by denaturing (7.5 M urea) 6% PAGE for biosensor characterization and use in quantitative assays. RNAs purified from PAGE were subsequently extracted from gel pieces using Crush Soak buffer (10 mM Tris-HCl [pH 7.5], 200 mM NaCl, and 1 mM EDTA [pH 8.0]). RNAs were precipitated with ethanol, dried, and then resuspended in TE buffer (10 mM Tris-HCl [pH 8.0] and 1 mM EDTA). Accurate measurement of RNA concentration was determined by measuring the absorbance at 260 nm after performing a hydrolysis assay to eliminate the hypochromic effect due to the secondary structure in these RNAs (Wilson et al., 2014).

Expression and Purification of cGAS Enzyme

N-terminal 6xHis-MBP-tagged full-length cGAS encoding plasmid was donated by the Doudna lab (Kranzusch et al., 2013). Protein expression was induced in *Escherichia coli* BL21-RIL DE3 along with pRARE2 human tRNA plasmid (Agilent) with addition of 0.5 M isopropyl-thio-β-D-galactoside to Luria-Bertani media for 20 hr at 16°C. Cells were lysed by sonication in 20 mM HEPES (pH 7.5), 400 mM NaCl, 10% glycerol, 30 mM imidazole, 1 mM PMSF, and 1 mM Tris(2-carboxyethy1)phosphine (TCEP). The lysate was treated with DNase (Worthington Biochemical) for 30 min to remove residual DNA bound to cGAS. Clarified lysate was bound to Ni-NTA agarose (QIAGEN) and was washed with lysis buffer supplemented with 1 M NaCl. The bound protein was eluted using lysis buffer supplemented with 300 mM imidazole. The eluted protein was dialyzed overnight at 4°C in buffer having 20 mM HEPES (pH 7.5), 150 mM KCl, 10% glycerol, and 1 mM TCEP.

TLC Assay of cGAS Activity

Enzyme activity of recombinant full-length cGAS was assayed in buffer containing 40 mM Tris-HCl (pH 7.5), 100 mM NaCl, and 10 mM $MgCl_2$ (Sigma-Aldrich). cGAS (estimated final concentration 1.5 μM) or equal volume of water was incubated with activating ligand HT-DNA (final concentration 0.1 mg/mL) in the presence of 250 μM ATP, 250 μM GTP, and trace amounts of [α-^{32}P]ATP or [α-^{32}P]GTP (~30 nM) at 37°C for 1.5 hr. Reactions were terminated with addition of 5 U of alkaline phosphatase (New England Biolabs) and further incubation at 37°C for 30 min. One microliter of each reaction was spotted onto a PEI-Cellulose F TLC plate (EMD Millipore), and reaction products were separated with the use of 1.5 M KH_2PO_4 (pH 3.8) as solvent. Plates were dried and radiolabeled products were detected by imaging the exposed phosphor screen using a Typhoon phosphorimager (GE Healthcare).

General Procedure for In Vitro Fluorescence Assays

In vitro fluorescence assays were carried out in a buffer containing 40 mM HEPES (pH 7.5 and 125) mM KCl. Other conditions, including temperature, concentration of $MgCl_2$, DFHBI (or DFHBI-1T), ligand (or cell extract), and RNA were varied in different experiments and are indicated in the figures. The RNA was renatured in buffer at 70°C for 3 min and cooled to ambient temperature for 5 min prior to addition to the reaction solution containing DFHBI (or DFHBI-1T), buffer, and ligand. Binding reactions were performed either in 100 μL (96-well plate) or 30 μL (384-well plate) volumes and were incubated at the indicated temperature in either a Corning Costar 3915 96-well black plate or a Greiner 781077 384-well black plate until equilibrium was reached, which typically takes 30 to 60 min. The fluorescence emission was measured using a Molecular Devices SpectraMax Paradigm Multi-Mode detection platform plate reader with the following instrument parameters: 448 nm excitation, 506 nm emission for DFHBI or 470 nm excitation, 510 nm emission for DFHBI-1T.

cGAS Activity and Inhibition Assay

To initiate the enzyme reaction, 0.5 μL of HT-DNA was added to 2.5 μL of 6× enzyme reaction solution containing cGAS, GTP, ATP, and reaction buffer. In general, final concentrations are 100 μg/mL HT-DNA, 1.5 μM cGAS, 200 μM GTP, and 200 μM ATP in enzyme reaction buffer (40 mM Tris-HCl [pH 7.5], 100 mM NaCl, and 10 mM $MgCl_2$). The enzyme reactions are incubated at

37°C for 2 hr. For the inhibition assay shown in Figure S2B, the reaction conditions are the same as described above except various concentrations of quinacrine was added.

To initiate the fluorescent biosensor reaction, 3 μL of the enzyme reaction was added to 27 μL of biosensor reaction solution containing renatured RNA, DFHBI (or DFHBI-1T), and biosensor binding buffer. Final concentrations are 200 nM RNA, 10 μM DFHBI (or DFHBI-1T), 40 mM HEPES (pH 7.5), 125 mM KCl, 10 mM $MgCl_2$, and 0.1× enzyme reaction buffer (4 mM Tris-HCl [pH 7.5], 10 mM NaCl, and 1 mM $MgCl_2$). Fluorescence measurements were conducted as described above. For the inhibition assay, due to the intrinsic fluorescence of quinacrine, DFHBI-1T was used to decrease overlap in its excitation wavelength. Samples containing only quinacrine at various concentrations in the biosensor binding buffer were used for background fluorescence subtraction.

HTS Assay of cGAS Activity

For HTS experiments, reaction component samples were dispensed into a Grenier 781077 384-well flat-bottom black plate using an Eppendorf Repeater Xstream pipetter. Z′ factors were calculated from 16-well replicates in the 384-well plate. For the cGAS activity assay, 0.5 μL of HT-DNA or water was added to 2.5 μL of reaction solution containing cGAS, GTP, ATP, and cGAS reaction buffer in each 0.2 mL PCR tube in two 8-tube strips (Bio-Rad). Final concentrations are: 100 μg/mL HT-DNA, 1.5 μM cGAS, 200 μM GTP, 200 μM ATP, and enzyme reaction buffer (40 mM Tris-HCl [pH 7.5], 100 mM NaCl, and 10 mM $MgCl_2$). After 2 hr incubation at 37°C, to initiate the fluorescent biosensor reaction, the total reaction solution (3 μL) was added in each well of the 384-well plate to 27 μL of biosensor assay solution containing renatured RNA, DFHBI, and biosensor binding buffer. Final concentrations are 200 nM RNA, 10 μM DFHBI, 40 mM HEPES (pH 7.5), 125 mM KCl, 10 mM $MgCl_2$, and 0.1× cGAS reaction buffer (4 mM Tris-HCl [pH 7.5], 10 mM NaCl, and 1 mM $MgCl_2$). Fluorescence measurements were conducted as described above.

Biosensor-Based Determination of 2′,3′-cGAMP Concentration in Mammalian Cell Extracts

L929 and HEK293T cells were maintained in DMEM medium with 10% fetal bovine serum in a humidified incubator at 37°C and 5% CO_2. To introduce cytosolic DNA, transfections were performed using Lipofectamine 2000 (Invitrogen) using the manufacturer's protocol. Typically, cells were seeded in 175 cm flasks at 90% confluence (2×10^6 cells) in 25 mL of medium. The Lipofectamine (125 μL) was mixed with 250 μg of HT-DNA (10 μg/mL) or no HT-DNA (mock) in Opti-MEM to a final volume of 200 μL and incubated at room temperature for 30 min. The transfection mixture was added to the cell culture and incubated for 6 hr, then cyclic dinucleotides were extracted from three 175 cm flasks of cells (~6×10^6 cells, quantified in a Neubauer chamber using a bright field microscope) after brief trypsinization to detach them from the flask. The extraction procedure was performed as described in the section on *E. coli* cell lysates. Mammalian cell lysates were concentrated to a final volume of 30 μL using a vacuum concentrator and used immediately or stored at −20°C.

To initiate the fluorescent biosensor reactions, 2 μL (1×), 5 μL (2.5×), or 10 μL (5×) of cell extracts (stimulated or non-stimulated) was added to a reaction solution adjusted to a final volume of 30 μL. Final concentrations are 200 nM RNA, 25 μM DFHBI-1T, 40 mM HEPES (pH 7.5), 125 mM KCl, and 10 mM $MgCl_2$. Fluorescence measurements were conducted as described above. For experiments with SVPD, active (200 μU) or heat-inactivated SVPD (95°C for 5 min) was added to 2 μL (1× cell lysate) of cell extract and incubated at 37°C for 1 hr. The reactions were stopped by heating at 95°C for 5 min, rapidly cooled on ice, and then analyzed in fluorescent biosensor reactions.

To generate a standard fluorescence response curve in L929 cell lysates, known concentrations of commercial 2′,3′-cGAMP in water were mixed with 1 μL of non-stimulated cell extract, followed by addition to a reaction solution adjusted to a final volume of 25 μL. See Supplemental Experimental Procedures for details on calculation.

SUPPLEMENTAL INFORMATION

Supplemental Information includes Supplemental Experimental Procedures, four figures, and two tables and can be found with this article online at http://dx.doi.org/10.1016/j.chembiol.2016.10.014.

AUTHOR CONTRIBUTIONS

D.B., Y.S., and M.C.H. designed the research; D.B. and Y.S. conducted the experiments; A.M. contributed the new reagents; D.B., Y.S., A.M., D.R., and M.C.H. analyzed the data; and D.B., Y.S., and M.C.H. wrote the paper.

ACKNOWLEDGMENTS

We thank Philipp Kranzusch from the Doudna laboratory at the University of California, Berkeley, for providing the 6xHis-MBP-cGAS plasmid. This work was also supported by NIH DP2 OD008677 (to M.C.H.), NIH R01 AI113041 (to D.R.), Cancer Research Coordinating Committee (CRCC) predoctoral fellowship (to Y.S.), and NIH Training Grant T32 GM066698 (for Y.S.). D.H.R. is a member of the scientific advisory board of and receives research funding from Aduro Biotech.

Received: July 18, 2016
Revised: September 2, 2016
Accepted: October 25, 2016
Published: November 23, 2016

REFERENCES

Ablasser, A., Goldeck, M., Cavlar, T., Deimling, T., Witte, G., Rohl, I., Hopfner, K.P., Ludwig, J., and Hornung, V. (2013). cGAS produces a 2′-5′-linked cyclic dinucleotide second messenger that activates STING. Nature *498*, 380–384.

Ahn, J., Gutman, D., Saijo, S., and Barber, G.N. (2012). STING manifests self DNA-dependent inflammatory disease. Proc. Natl. Acad. Sci. USA *109*, 19386–19391.

Ahn, J., Ruiz, P., and Barber, G.N. (2014). Intrinsic self-DNA triggers inflammatory disease dependent on STING. J. Immunol. *193*, 4634–4642.

Ahn, J., Konno, H., and Barber, G.N. (2015). Diverse roles of STING-dependent signaling on the development of cancer. Oncogene *34*, 5302–5308.

An, J., Woodward, J.J., Sasaki, T., Minie, M., and Elkon, K.B. (2015). Cutting edge: antimalarial drugs inhibit IFN-beta production through blockade of cyclic GMP-AMP synthase-DNA interaction. J. Immunol. *194*, 4089–4093.

Baird, J.R., Friedman, D., Cottam, B., Dubensky, T.W., Jr., Kanne, D.B., Bambina, S., Bahjat, K., Crittenden, M.R., and Gough, M.J. (2016). Radiotherapy combined with novel STING-targeting oligonucleotides results in regression of established tumors. Cancer Res. *76*, 50–61.

Barker, J.R., Koestler, B.J., Carpenter, V.K., Burdette, D.L., Waters, C.M., Vance, R.E., and Valdivia, R.H. (2013). STING-dependent recognition of cyclic di-AMP mediates type I interferon responses during *Chlamydia trachomatis* infection. MBio *4*, e00018-13.

Boer, D.R., Canals, A., and Coll, M. (2009). DNA-binding drugs caught in action: the latest 3D pictures of drug-DNA complexes. Dalton Trans. 399–414.

Burdette, D.L., Monroe, K.M., Sotelo-Troha, K., Iwig, J.S., Eckert, B., Hyodo, M., Hayakawa, Y., and Vance, R.E. (2011). STING is a direct innate immune sensor of cyclic di-GMP. Nature *478*, 515–518.

Burhenne, H., and Kaever, V. (2013). Quantification of cyclic dinucleotides by reversed-phase LC-MS/MS. Methods Mol. Biol. *1016*, 27–37.

Chandra, D., Quispe-Tintaya, W., Jahangir, A., Asafu-Adjei, D., Ramos, I., Sintim, H.O., Zhou, J., Hayakawa, Y., Karaolis, D.K., and Gravekamp, C. (2014). STING ligand c-di-GMP improves cancer vaccination against metastatic breast cancer. Cancer Immunol. Res. *2*, 901–910.

Corrales, L., and Gajewski, T.F. (2015). Molecular pathways: targeting the stimulator of interferon genes (STING) in the immunotherapy of cancer. Clin. Cancer Res. *21*, 4774–4779.

Corrales, L., Glickman, L.H., McWhirter, S.M., Kanne, D.B., Sivick, K.E., Katibah, G.E., Woo, S.R., Lemmens, E., Banda, T., Leong, J.J., et al. (2015). Direct activation of STING in the tumor microenvironment leads to potent and systemic tumor regression and immunity. Cell Rep. *11*, 1018–1030.

Curran, E., Corrales, L., and Kline, J. (2015). Targeting the innate immune system as immunotherapy for acute myeloid leukemia. Front. Oncol. *5*, 83.

Demaria, O., De Gassart, A., Coso, S., Gestermann, N., Di Domizio, J., Flatz, L., Gaide, O., Michielin, O., Hwu, P., Petrova, T.V., et al. (2015). STING activation of tumor endothelial cells initiates spontaneous and therapeutic antitumor immunity. Proc. Natl. Acad. Sci. USA *112*, 15408–15413.

Deng, L., Liang, H., Xu, M., Yang, X., Burnette, B., Arina, A., Li, X.D., Mauceri, H., Beckett, M., Darga, T., et al. (2014). STING-dependent cytosolic DNA sensing promotes radiation-induced type I interferon-dependent antitumor immunity in immunogenic tumors. Immunity *41*, 843–852.

Diner, E.J., Burdette, D.L., Wilson, S.C., Monroe, K.M., Kellenberger, C.A., Hyodo, M., Hayakawa, Y., Hammond, M.C., and Vance, R.E. (2013). The innate immune DNA sensor cGAS produces a noncanonical cyclic dinucleotide that activates human STING. Cell Rep. *3*, 1355–1361.

Downey, C.M., Aghaei, M., Schwendener, R.A., and Jirik, F.R. (2014). DMXAA causes tumor site-specific vascular disruption in murine non-small cell lung cancer, and like the endogenous non-canonical cyclic dinucleotide STING agonist, 2′3′-cGAMP, induces M2 macrophage repolarization. PLoS One *9*, e99988.

Gao, D., Wu, J., Wu, Y.T., Du, F., Aroh, C., Yan, N., Sun, L., and Chen, Z.J. (2013a). Cyclic GMP-AMP synthase is an innate immune sensor of HIV and other retroviruses. Science *341*, 903–906.

Gao, P., Ascano, M., Wu, Y., Barchet, W., Gaffney, B.L., Zillinger, T., Serganov, A.A., Liu, Y., Jones, R.A., Hartmann, G., et al. (2013b). Cyclic [G(2′,5′)pA(3′,5′)p] is the metazoan second messenger produced by DNA-activated cyclic GMP-AMP synthase. Cell *153*, 1094–1107.

Gao, D., Li, T., Li, X.D., Chen, X., Li, Q.Z., Wight-Carter, M., and Chen, Z.J. (2015). Activation of cyclic GMP-AMP synthase by self-DNA causes autoimmune diseases. Proc. Natl. Acad. Sci. USA *112*, E5699–E5705.

Hansen, K., Prabakaran, T., Laustsen, A., Jorgensen, S.E., Rahbaek, S.H., Jensen, S.B., Nielsen, R., Leber, J.H., Decker, T., Horan, K.A., et al. (2014). Listeria monocytogenes induces IFNbeta expression through an IFI16-, cGAS- and STING-dependent pathway. EMBO J. *33*, 1654–1666.

Herzner, A.M., Hagmann, C.A., Goldeck, M., Wolter, S., Kubler, K., Wittmann, S., Gramberg, T., Andreeva, L., Hopfner, K.P., Mertens, C., et al. (2015). Sequence-specific activation of the DNA sensor cGAS by Y-form DNA structures as found in primary HIV-1 cDNA. Nat. Immunol. *16*, 1025–1033.

Hossain, M., Giri, P., and Kumar, G.S. (2008). DNA intercalation by quinacrine and methylene blue: a comparative binding and thermodynamic characterization study. DNA Cell Biol *27*, 81–90.

Ishikawa, H., and Barber, G.N. (2008). STING is an endoplasmic reticulum adaptor that facilitates innate immune signalling. Nature *455*, 674–678.

Kellenberger, C.A., and Hammond, M.C. (2015). In vitro analysis of riboswitch-Spinach aptamer fusions as metabolite-sensing fluorescent biosensors. Methods Enzymol. *550*, 147–172.

Kellenberger, C.A., Wilson, S.C., Sales-Lee, J., and Hammond, M.C. (2013). RNA-based fluorescent biosensors for live cell imaging of second messengers cyclic di-GMP and cyclic AMP-GMP. J. Am. Chem. Soc. *135*, 4906–4909.

Kellenberger, C.A., Wilson, S.C., Hickey, S.F., Gonzalez, T.L., Su, Y., Hallberg, Z.F., Brewer, T.F., Iavarone, A.T., Carlson, H.K., Hsieh, Y.F., et al. (2015). GEMM-I riboswitches from Geobacter sense the bacterial second messenger cyclic AMP-GMP. Proc. Natl. Acad. Sci. USA *112*, 5383–5388.

Kobayashi, H., Kobayashi, C.I., Nakamura-Ishizu, A., Karigane, D., Haeno, H., Yamamoto, K.N., Sato, T., Ohteki, T., Hayakawa, Y., Barber, G.N., et al. (2015). Bacterial c-di-GMP affects hematopoietic stem/progenitors and their niches through STING. Cell Rep. *11*, 71–84.

Kranzusch, P.J., Lee, A.S., Berger, J.M., and Doudna, J.A. (2013). Structure of human cGAS reveals a conserved family of second-messenger enzymes in innate immunity. Cell Rep. *3*, 1362–1368.

Lee, E.R., Baker, J.L., Weinberg, Z., Sudarsan, N., and Breaker, R.R. (2010). An allosteric self-splicing ribozyme triggered by a bacterial second messenger. Science *329*, 845–848.

LePecq, J.B., and Paoletti, C. (1967). A fluorescent complex between ethidium bromide and nucleic acids. Physical-chemical characterization. J. Mol. Biol. *27*, 87–106.

Li, X., Shu, C., Yi, G., Chaton, C.T., Shelton, C.L., Diao, J., Zuo, X., Kao, C.C., Herr, A.B., and Li, P. (2013). Cyclic GMP-AMP synthase is activated by double-stranded DNA-induced oligomerization. Immunity *39*, 1019–1031.

Li, T., Cheng, H., Yuan, H., Xu, Q., Shu, C., Zhang, Y., Xu, P., Tan, J., Rui, Y., Li, P., et al. (2016). Antitumor activity of cGAMP via stimulation of cGAS-cGAMP-STING-IRF3 mediated innate immune response. Sci. Rep. *6*, 19049.

Ma, Z., and Damania, B. (2016). The cGAS-STING defense pathway and its counteraction by viruses. Cell Host Microbe *19*, 150–158.

Nakamura, T., Miyabe, H., Hyodo, M., Sato, Y., Hayakawa, Y., and Harashima, H. (2015). Liposomes loaded with a STING pathway ligand, cyclic di-GMP, enhance cancer immunotherapy against metastatic melanoma. J. Control. Release *216*, 149–157.

Paijo, J., Doring, M., Spanier, J., Grabski, E., Nooruzzaman, M., Schmidt, T., Witte, G., Messerle, M., Hornung, V., Kaever, V., et al. (2016). cGAS senses human cytomegalovirus and induces type I interferon responses in human monocyte-derived cells. PLoS Pathog. *12*, e1005546.

Ren, A., Wang, X.C., Kellenberger, C.A., Rajashankar, K.R., Jones, R.A., Hammond, M.C., and Patel, D.J. (2015). Structural basis for molecular discrimination by a 3′,3′-cGAMP sensing riboswitch. Cell Rep. *11*, 1–12.

Shanahan, C.A., Gaffney, B.L., Jones, R.A., and Strobel, S.A. (2011). Differential analogue binding by two classes of c-di-GMP riboswitches. J. Am. Chem. Soc. *133*, 15578–15592.

Shrivastav, M., and Niewold, T.B. (2013). Nucleic acid sensors and type I interferon production in systemic lupus erythematosus. Front. Immunol. *4*, 319.

Sinha, R., Hossain, M., and Kumar, G.S. (2007). RNA targeting by DNA binding drugs: structural, conformational and energetic aspects of the binding of quinacrine and DAPI to A-form and H(L)-form of poly(rC).poly(rG). Biochim. Biophys. Acta *1770*, 1636–1650.

Smith, K.D., Shanahan, C.A., Moore, E.L., Simon, A.C., and Strobel, S.A. (2011). Structural basis of differential ligand recognition by two classes of bis-(3′-5′)-cyclic dimeric guanosine monophosphate-binding riboswitches. Proc. Natl. Acad. Sci. USA *108*, 7757–7762.

Song, W., Strack, R.L., Svensen, N., and Jaffrey, S.R. (2014). Plug-and-play fluorophores extend the spectral properties of Spinach. J. Am. Chem. Soc. *136*, 1198–1201.

Su, Y., Hickey, S.F., Keyser, S.G., and Hammond, M.C. (2016). In vitro and in vivo enzyme activity screening via RNA-based fluorescent biosensors for S-adenosyl-l-homocysteine (SAH). J. Am. Chem. Soc. *138*, 7040–7047.

Sun, L., Wu, J., Du, F., Chen, X., and Chen, Z.J. (2013). Cyclic GMP-AMP synthase is a cytosolic DNA sensor that activates the type I interferon pathway. Science *339*, 786–791.

Svensen, N., and Jaffrey, S.R. (2016). Fluorescent RNA aptamers as a tool to study RNA-modifying enzymes. Cell Chem Biol. *23*, 415–425.

Wang, X.C., Stephen, C.W., and Hammond, M.C. (2016). Next-generation RNA-based fluorescent biosensors enable anaerobic detection of cyclic di-GMP. Nucleic Acids Res. *44*, e139.

Waters, C.M. (2010). Methods for cyclic di-GMP detection. In The Second Messenger Cyclic Di-GMP, A.J. Wolfe and K.L. Visick, eds. (ASM Press), pp. 68–75.

Watson, R.O., Bell, S.L., MacDuff, D.A., Kimmey, J.M., Diner, E.J., Olivas, J., Vance, R.E., Stallings, C.L., Virgin, H.W., and Cox, J.S. (2015). The cytosolic sensor cGAS detects mycobacterium tuberculosis DNA to induce type I interferons and activate autophagy. Cell Host Microbe *17*, 811–819.

Wheate, N.J., Brodie, C.R., Collins, J.G., Kemp, S., and Aldrich-Wright, J.R. (2007). DNA intercalators in cancer therapy: organic and inorganic drugs and their spectroscopic tools of analysis. Mini Rev. Med. Chem. *7*, 627–648.

White, M.J., McArthur, K., Metcalf, D., Lane, R.M., Cambier, J.C., Herold, M.J., van Delft, M.F., Bedoui, S., Lessene, G., Ritchie, M.E., et al. (2014). Apoptotic caspases suppress mtDNA-induced STING-mediated type I IFN production. Cell *159*, 1549–1562.

Wilson, S.C., Cohen, D.T., Wang, X.C., and Hammond, M.C. (2014). A neutral pH thermal hydrolysis method for quantification of structured RNAs. RNA *20*, 1153–1160.

Woo, S.R., Fuertes, M.B., Corrales, L., Spranger, S., Furdyna, M.J., Leung, M.Y., Duggan, R., Wang, Y., Barber, G.N., Fitzgerald, K.A., et al. (2014). STING-dependent cytosolic DNA sensing mediates innate immune recognition of immunogenic tumors. Immunity *41*, 830–842.

Woo, S.R., Corrales, L., and Gajewski, T.F. (2015a). Innate immune recognition of cancer. Annu. Rev. Immunol. *33*, 445–474.

Woo, S.R., Corrales, L., and Gajewski, T.F. (2015b). The STING pathway and the T cell-inflamed tumor microenvironment. Trends Immunol. *36*, 250–256.

Wu, J., Sun, L., Chen, X., Du, F., Shi, H., Chen, C., and Chen, Z.J. (2013). Cyclic GMP-AMP is an endogenous second messenger in innate immune signaling by cytosolic DNA. Science *339*, 826–830.

Wu, M.C., Lowe, P.T., Robinson, C.J., Vincent, H.A., Dixon, N., Leigh, J., and Micklefield, J. (2015). Rational re-engineering of a transcriptional silencing PreQ1 riboswitch. J. Am. Chem. Soc. *137*, 9015–9021.

Zhang, J.H., Chung, T.D., and Oldenburg, K.R. (1999). A simple statistical parameter for use in evaluation and validation of high throughput screening assays. J. Biomol. Screen. *4*, 67–73.

Zhang, X., Shi, H., Wu, J., Zhang, X., Sun, L., Chen, C., and Chen, Z.J. (2013). Cyclic GMP-AMP containing mixed phosphodiester linkages is an endogenous high-affinity ligand for STING. Mol. Cell *51*, 226–235.

Zhang, H., Tang, K., Zhang, Y., Ma, R., Ma, J., Li, Y., Luo, S., Liang, X., Ji, T., Gu, Z., et al. (2015). Cell-free tumor microparticle vaccines stimulate dendritic cells via cGAS/STING signaling. Cancer Immunol. Res. *3*, 196–205.

Cell Chemical Biology, Volume *23*

Supplemental Information

An RNA-Based Fluorescent Biosensor for High-Throughput Analysis of the cGAS-cGAMP-STING Pathway

Debojit Bose, Yichi Su, Assaf Marcus, David H. Raulet, and Ming C. Hammond

Supplemental Information

for

An RNA-based fluorescent biosensor for high-throughput analysis of the cGAS-cGAMP-STING pathway

Debojit Bose*, Yichi Su*, Assaf Marcus,
David Raulet, Ming C. Hammond

*These authors contributed equally to the work

Table of contents

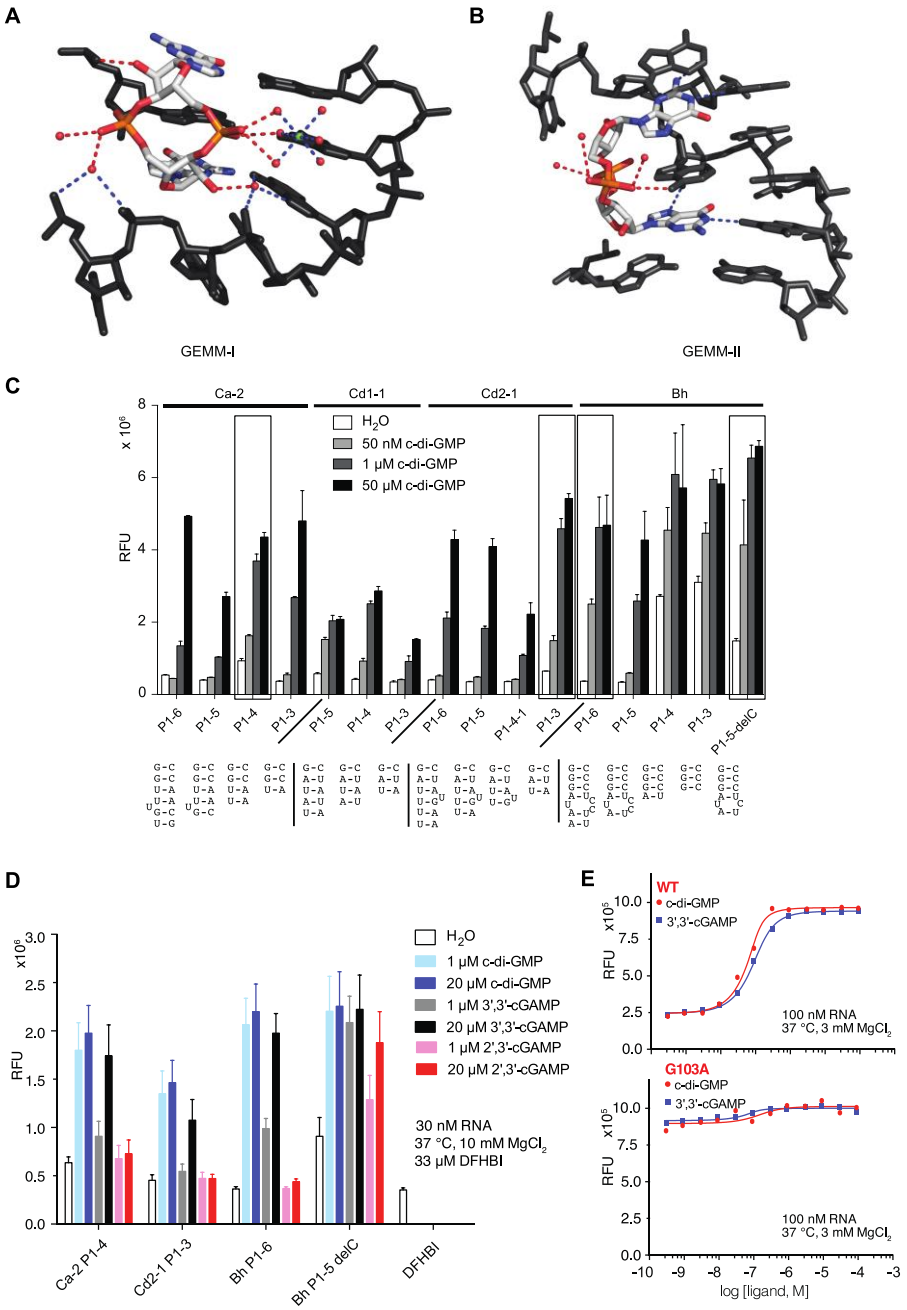

Figure S1 (related to Figure 1). Screen and mutagenesis analysis for GEMM-II riboswitch-based 2′, 3′-cGAMP biosensors.

Interactions between (A) GEMM-I riboswitch (PDB code 3MXH) or (B) GEMM-II riboswitch (PDB code 3Q3Z) with 2′-hydroxyls and phosphodiester oxygens of c-di-GMP. The interactions are shown in red dashes. (C) Screening of different phylogenetic and stem varients of GEMM-II riboswitch for developing 2′, 3′-cGAMP biosensor. Error-bars represent the standard deviation of 3 independent replicates. (D) Analysis of biosensor hits from screening in (C) for their response to different cylic dinucloetides. (E) Selectivity profiles of Bh P1-5 delC WT and G103A biosensors, *in vitro* fluorescence activation and binding affinity measurements for Bh P1-5 delC variants with bacterial cyclic dinucleotides, c-di-GMP and 3′,3′-cGAMP. Error bars indicate standard deviations for three independent replicates.

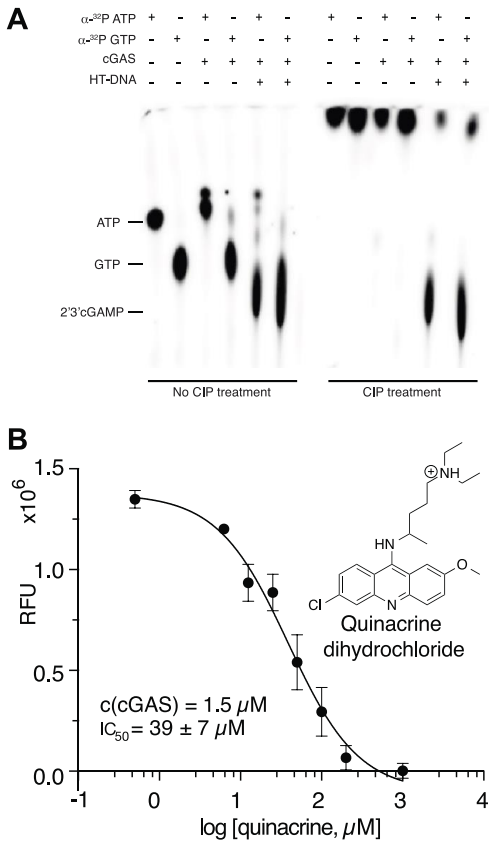

Figure S2 (related to Figure 2, Figure 3). TLC-based cGAS activity assay and RNA biosensor-based cGAS inhibition assay.
(A) TLC-based assay with radiolabeled substrates to assess cGAS activity. Calf intestinal alkaline phosphatase (CIP) was used to remove free nucleotide triphosphate. Image is representative of multiple independent experiments. (B) Initial analysis of cGAS inhibition by quinacrine (QC) via RNA-based fluorescent biosensor. The determined IC_{50} was later revealed to be artefactual due to the intercalating effect of QC to the RNA-based biosensor. Error bars indicate standard deviations for three independent replicates.

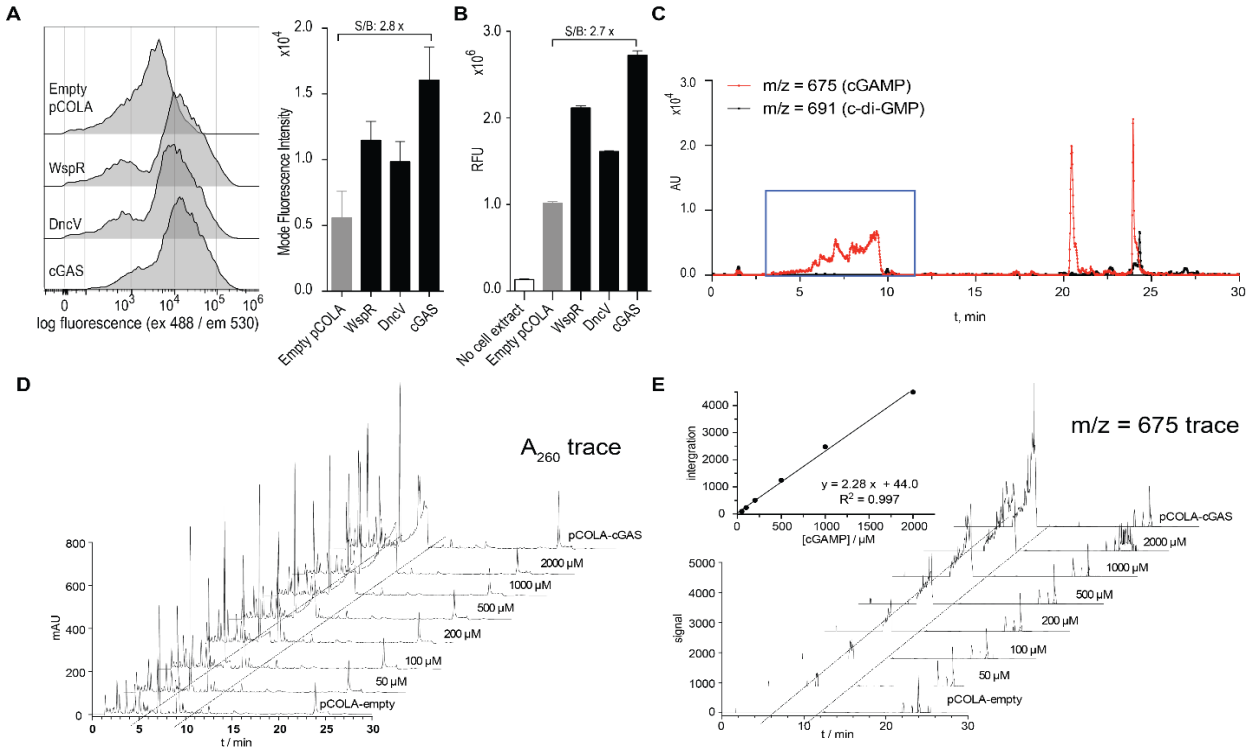

Figure S3 (related to Figure 4). Application of fluorescent biosensor to detect 3',3'-cGAMP and other cyclic dinucleotides in bacterial cells expressing synthase enzymes.
(A) Representative flow cytometry analysis of live *E. coli* expressing plasmids encoding both biosensor and cyclic dinucleotide synthases after incubation in media containing DFHBI-1T. Fluorescence values on x-axis are shown using HyperLog scaling. The average mode fluorescence intensity (MFI) from two independent biological replicates are shown in the bar graph, error bars depict standard deviations. (B) *In vitro* fluorescence biosensor-based analysis of cyclic dinucleotide content of cell extracts from *E. coli* expressing the corresponding cyclic dinucleotide synthases. Error bars depict standard deviations for two independent biological replicates. (C) LC-MS analysis of cell extract from *E. coli* expressing a plasmid encoding cGAS. Mass trace corresponding to 2′,3′-cGAMP (m/z = 675, red) and c-di-GMP (m/z = 691, blue) were shown. Signal peaks corresponding to 2′,3′-cGAMP production were boxed. (D, E) Quantitation of 2′, 3′-cGAMP in *E. coli* expressing a plasmid encoding cGAS. Cell extracts from *E. coli* expressing an empty pCOLA vector plasmid was added with varied concentrations of 2′, 3′-cGAMP and then assayed by LC-MS, with 260 nm absorbance (D) and mass spec signal (E) shown. Standard curve for quantifying 2′, 3′-cGAMP based on the integration of mass spec signal was shown in inset in (E). All the data were collected on an Agilent 1260 Infinity LC-MS system equipped with a Poroshell 120 C-18 column. Error bars indicate standard deviations for three independent replicates.

Measuring activity of expressed cGAS in live bacterial cells
Prior work in our lab has established riboswitch-based biosensors for metabolite detection in live *E. coli* (Hallberg et al., 2016; Kellenberger et al., 2015a; Kellenberger et al., 2015c; Kellenberger et al., 2013; Su et al., 2016), so we were interested to benchmark the performance of the 2′, 3′-cGAMP biosensor under similar *in vivo* conditions. In order to test this, we inserted the biosensor construct into the tRNA scaffold (Kellenberger et al., 2015b; Ponchon and Dardel, 2007), then co-expressed the fluorescent biosensor along with empty vector or enzymes that synthesize different cyclic dinucleotides in *E. coli* BL21-Star cells. WspR from *Pseudomonas fluorescens* produces c-di-GMP, DncV from *Vibrio cholerae* produces 3′, 3′-cGAMP, and cGAS from *Homo sapiens* produces 2′, 3′-cGAMP. After incubating cells with the profluorescent dye DFHBI-1T (Song et al., 2014), the cellular fluorescence was analyzed by flow cytometry, which provides high-throughput, single-cell quantitation of metabolites as detected by the fluorescent biosensor. The heterogeneity observed in the fluorescence values for a cell population is attributed to differences in multiple factors in the experiment, such as plasmid copy number, enzyme expression level, RNA biosensor expression level, and cell size in live, replicating *E. coli*. To address this issue, the mode fluorescence intensity (MFI, defined as the value with

the most observations) of each population was analyzed since this value was consistent between independent biological replicates.

As expected, significant fluorescence activation was observed upon co-expression of each enzyme (Fig. S3A), because the Bh P1-6 G103A biosensor is capable of binding 3′, 3′-cGAMP, c-di-GMP, and 2′, 3′-cGAMP (listed in order of affinity). However, the degree of fluorescence activation did not correspond to the relative affinity of the biosensors for the different cyclic dinucleotides. Instead, it appears to correlate directly to the amount of each cyclic dinucleotide produced by the enzymes *in vivo*, as the identical trend was observed when we performed an aqueous-organic extraction of cell lysates and analyzed the extracts containing cyclic dinucleotides using the biosensor (Fig. S3B). Notably, given that the biosensor has poorer affinity for 2′, 3′-cGAMP versus the two 3′, 3′-linked cyclic dinucleotides, this result implies that cGAS is highly activated by binding to endogenous genomic DNA to produce an extremely large amount of 2′, 3′-cGAMP in *E. coli*. In addition, there is likely no endogenous phosphodiesterase capable of efficiently hydrolyzing the compound. Accordingly, LCMS analysis showed that 2′, 3′-cGAMP is highly abundant in the cell extracts, building up to ~0.5 mM concentration based on our standard curve (Fig. S3C, D, E). It should also be noted that *E. coli* has endogenous c-di-GMP (Weber et al., 2006), so basal activation is observed for cells harboring the empty pCOLA vector, both in vivo and in extracts. Thus, the fluorescence activation of the biosensor we observed is likely lower than the theoretical maximum fold activation if we compared to cells that have no c-di-GMP. For example, to our knowledge mammalian cells do not produce c-di-GMP, except for those engineered for synthetic biology applications (Folcher et al., 2014). In all, these live-cell flow cytometry results demonstrate that our first-generation biosensors are capable of detecting 2′,3′-cGAMP in the complex setting of bacterial cells, which lays the foundation for achieving 2′,3′-cGAMP detection in live mammalian cells.

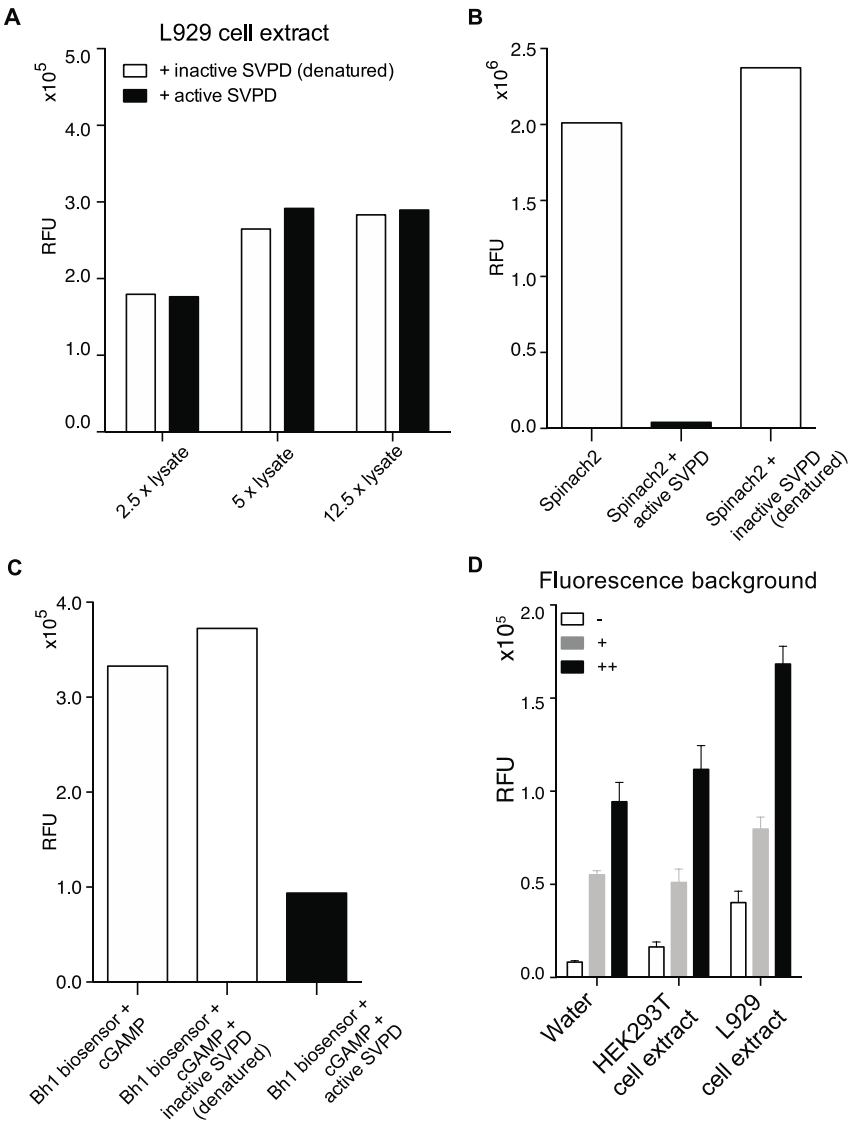

Figure S4 (related to Figure 4). Source of fluorescence background in biosensor-based analysis of mammalian cell extracts.

(A-C) SVPD degradation experiments to rule out basal 2′, 3′-cGAMP in L929 cells. (A) Fluorescence readings for varied concentration of mock-transfected L929 cell extracts treated with active or denatured SVPD prior to biosensor addition. (B) Fluorescence readings for Spinach2 aptamer treated with active or denatured SVPD. (C) Fluorescence readings for 2′,3′-cGAMP treated with active or denatured SVPD prior to biosensor addition. (D) The origin of background fluorescence in mock-stimulated cell extract was investigated. (-, cell extract alone; +, cell extract + DFHBI; ++, cell extract + biosensor + DFHBI.) Error bars indicate standard deviations for three independent biological replicates.

Table S1 (related to Figure 1). GEMM-II riboswitch-based biosensors sequences

Name	Sequences
Ca-2 P1-6	GATGTAACTGAATGAAATGGTGAAGGACGGGTCCA***TGTTTGG***AAACAATGAT GAATTTCTTTAAATTGGGCACTTGAGAAATTTTGAGTTAGTAGTGCAACCGA***C CAACG***TTGTTGAGTAGAGTGTGAGCTCCGTAACTAGTTACATC
Ca-2 P1-5	GATGTAACTGAATGAAATGGTGAAGGACGGGTCCA***GTTTGG***AAACAATGATG AATTTCTTTAAATTGGGCACTTGAGAAATTTTGAGTTAGTAGTGCAACCGA***CC AAC***TTGTTGAGTAGAGTGTGAGCTCCGTAACTAGTTACATC
Ca-2 P1-4	GATGTAACTGAATGAAATGGTGAAGGACGGGTCCA***TTGG***AAACAATGATGAA TTTCTTTAAATTGGGCACTTGAGAAATTTTGAGTTAGTAGTGCAACCGA***CCAA*** TTGTTGAGTAGAGTGTGAGCTCCGTAACTAGTTACATC
Ca-2 P1-3	GATGTAACTGAATGAAATGGTGAAGGACGGGTCCA***TGG***AAACAATGATGAAT TTCTTTAAATTGGGCACTTGAGAAATTTTGAGTTAGTAGTGCAACCGA***CCA***TT GTTGAGTAGAGTGTGAGCTCCGTAACTAGTTACATC
Cd1-1 P1-5	GATGTAACTGAATGAAATGGTGAAGGACGGGTCCA***TATAG***AAACTGTGAAGT ATATCTTAAACCTGGGCACTTAAAAGATATATGGAGTTAGTAGTGCAACCTG***C TATA***TTGTTGAGTAGAGTGTGAGCTCCGTAACTAGTTACATC
Cd1-1 P1-4	GATGTAACTGAATGAAATGGTGAAGGACGGGTCCA***ATAG***AAACTGTGAAGTA TATCTTAAACCTGGGCACTTAAAAGATATATGGAGTTAGTAGTGCAACCTG***CT AT***TTGTTGAGTAGAGTGTGAGCTCCGTAACTAGTTACATC
Cd1-1 P1-3	GATGTAACTGAATGAAATGGTGAAGGACGGGTCCA***TAG***AAACTGTGAAGTAT ATCTTAAACCTGGGCACTTAAAAGATATATGGAGTTAGTAGTGCAACCTG***CT A***TTGTTGAGTAGAGTGTGAGCTCCGTAACTAGTTACATC
Cd2-1 P1-6	GATGTAACTGAATGAAATGGTGAAGGACGGGTCCA***TTTTAG***AAACTGAGAAG TATATCTTATTATTGGGCATCTGGAGATATATGGAGTTAGTGGTGCAACCGG ***CTATGAA***TTGTTGAGTAGAGTGTGAGCTCCGTAACTAGTTACATC
Cd2-1 P1-5	GATGTAACTGAATGAAATGGTGAAGGACGGGTCCA***TTTAG***AAACTGAGAAGT ATATCTTATTATTGGGCATCTGGAGATATATGGAGTTAGTGGTGCAACCGG***C TATGA***TTGTTGAGTAGAGTGTGAGCTCCGTAACTAGTTACATC
Cd2-1 P1-4	GATGTAACTGAATGAAATGGTGAAGGACGGGTCC***TTAG***AAACTGAGAAGTAT ATCTTATTATTGGGCATCTGGAGATATATGGAGTTAGTGGTGCAACCGG***CTA TG***TTGTTGAGTAGAGTGTGAGCTCCGTAACTAGTTACATC
Cd2-1 P1-3	GATGTAACTGAATGAAATGGTGAAGGACGGGTCC***TAG***AAACTGAGAAGTATA TCTTATTATTGGGCATCTGGAGATATATGGAGTTAGTGGTGCAACCGG***CTA***T TGTTGAGTAGAGTGTGAGCTCCGTAACTAGTTACATC
Bh P1-6	GATGTAACTGAATGAAATGGTGAAGGACGGGTCC***AATAGGG***AAGCAACGAA GCATAGCCTTTATATGGACACTTGGGTTATGTGGAGCTACTAGTGTAACCGG ***CCCTCCTT***TTGTTGAGTAGAGTGTGAGCTCCGTAACTAGTTACATC
Bh P1-5	GATGTAACTGAATGAAATGGTGAAGGACGGGTCC***ATAGGG***AAGCAACGAAG CATAGCCTTTATATGGACACTTGGGTTATGTGGAGCTACTAGTGTAACCGG***C CCTCCT***TTGTTGAGTAGAGTGTGAGCTCCGTAACTAGTTACATC
Bh P1-4	GATGTAACTGAATGAAATGGTGAAGGACGGGTCC***AGGG***AAGCAACGAAGCA TAGCCTTTATATGGACACTTGGGTTATGTGGAGCTACTAGTGTAACCGG***CCC T***TTGTTGAGTAGAGTGTGAGCTCCGTAACTAGTTACATC
Bh P1-3	GATGTAACTGAATGAAATGGTGAAGGACGGGTCC***GGG***AAGCAACGAAGCAT AGCCTTTATATGGACACTTGGGTTATGTGGAGCTACTAGTGTAACCGG***CCC***T TGTTGAGTAGAGTGTGAGCTCCGTAACTAGTTACATC
Bh P1-5 delC	GATGTAACTGAATGAAATGGTGAAGGACGGGTCC***ATAGGG***AAGCAACGAAG CATAGCCTTTATATGGACACTTGGGTTATGTGGAGCTACTAGTGTAACCGG***C CCTCT***TTGTTGAGTAGAGTGTGAGCTCCGTAACTAGTTACATC

Ca: Bacteria Firmicutes Clostridia Clostridiales Clostridiaceae *Clostridium acetobutylicum* ATCC 824
Cd1: Bacteria Firmicutes Clostridia Clostridiales Clostridiaceae *Clostridium difficile* 630
Cd2: Bacteria Firmicutes Clostridia Clostridiales Clostridiaceae *Clostridium difficile* QCD- 32g58
Bh: Bacteria Firmicutes Bacillales Bacillaceae *Bacillus halodurans* C-125

Table S2 (related to Figure 1). GEMM-II biosensor binding affinities and fluorescent turn-on properties

	Bh P1-5delC		Bh P1-6 WT		Bh P1-6 G103A	
	Kd (μM)	Fold turn-on (S/B ratio)	Kd (μM)	Fold turn-on (S/B ratio)	Kd (μM)	Fold turn-on (S/B ratio)
c-di-GMP[b]	0.021 ± 0.008	-	0.056 ± 0.012	13.1x	>7	8.2x
3′, 3′-cGAMP[b]	-	-	>11	10.8x	0.8 ± 0.1	9.6x
2′, 3′-cGAMP[a]	13.4 ± 0.9	5.1x	-	-	>65	10.3x

[a]Fold turn-on (or signal-to-background ratio) measured with 200 nM RNA, 100 μM ligand in a 384-well plate
[b]Fold turn-on (or signal-to-background ratio) measured with 100 nM RNA, 100 μM ligand in a 384-well plate

Supplemental Experimental Procedures

Analysis of biosensor binding affinities

To measure the apparent binding affinities of 2′, 3′-cGAMP biosensors, fluorescence assays were performed with the following conditions: 37 °C, 3 mM $MgCl_2$, 200 nM RNA, and 10 μM DFHBI. The 2′, 3′-cGAMP concentration (c_{cGAMP}) was varied, and the fluorescence of the sample with DFHBI but no RNA was subtracted as background to determine relative fluorescence units (RFU). The ratio between the fraction of biosensor that is bound by 2′, 3′-cGAMP and the total 2′, 3′-cGAMP biosensor concentration is given as:

$$ratio\ bound = \frac{[RNA \cdot cGAMP \cdot DFHBI]}{c_{total\ RNA}} = \frac{F - F_{\min}}{F_{\max} - F_{\min}}$$

Thus, for each concentration of 2′, 3′-cGAMP, the fluorescence of its corresponding sample should be:

$$F = \frac{[RNA \cdot cGAMP \cdot DFHBI]}{c_{total\ RNA}} \times (F_{\max} - F_{\min}) + F_{\min}$$

where F_{min} is the fluorescence of the sample containing no 2′, 3′-cGAMP, while F_{max} is the fluorescence of the sample containing highest concentration of 2′, 3′-cGAMP (100 μM).

The apparent dissociation constants K_d were determined by least squares fitting to the following equation in Graphpad Prism software:

$$F = \frac{[RNA \cdot cGAMP \cdot DFHBI]}{c_{total\ RNA}} \times (F_{\max} - F_{\min}) + F_{\min} =$$
$$\left[\frac{c_{total\ RNA} + K_d + c_{cGAMP} - \sqrt{(c_{total\ RNA} + K_d + c_{cGAMP})^2 - 4 \times c_{total\ RNA} \times c_{cGAMP}}}{2 \times c_{total\ RNA}}\right] \times (F_{\max} - F_{\min}) + F_{\min}$$

Determination of 2′, 3′-cGAMP concentration in *E. coli* cells overexpressing cGAS

E. coli harboring either empty pCOLA vector or pCOLA containing cGAS, DncV, or WspR genes were induced with 1 mM IPTG for 4 h at 37 ºC in 3 mL LB media, then the cells were pelleted and dry weight was measured (0.68, 0.75, 0.53, and 0.62 g, respectively). Cyclic dinucleotides were extracted as described previously (Spangler et al., 2010), with the following modifications. Pelleted cells were frozen at -80 ºC overnight. Frozen cell pellets were thawed and resuspended in 1.4 mL extraction buffer (40% acetonitrile, 40% methanol and 20% ddH_2O). Resuspended cells were incubated at room temperature with mild agitation for 20 min. After centrifugation for 5 min at 13,200 rpm, the supernatant was carefully removed and stored on ice. The remaining pellet was extracted twice more as described, with 700 μL extraction solvent each time. The combined supernatants were evaporated to dryness by rotary evaporation and the dried material was resuspended in 300 μL ddH_2O. The extract was filtered through a 3 kDa MW cutoff Amicon Ultra-4 Protein Concentrator (Millipore) and used immediately or stored at -20 °C. To obtain a standard curve for quantifying 2′,3′-cGAMP, known concentrations of commercial 2′,3′-cGAMP were doped into extracts from cells expressing empty pCOLA to a final volume of 20 μL. The samples were analyzed by LC-MS and the 675 m/z ion traces (corresponding to 2′,3′-cGAMP) were determined. See SI for details on calculation.

To initiate the fluorescent biosensor reaction, 3 μL of the bacterial cell extract was added to 27 μL of biosensor assay solution containing renatured RNA, DFHBI-1T, and biosensor binding buffer. Final concentrations are 200 nM RNA, 25 μM DFHBI-1T, 40 mM HEPES, pH 7.5, 125 mM KCl, and 10 mM $MgCl_2$. Fluorescence measurements were conducted as described above.

***In vivo* fluorescence assays by flow cytometry**

Preparation of cell samples for flow cytometry was carried out by inoculating 3 mL of LB media (containing carbenicillin and kanamycin) with 150 μL of an overnight culture of BL21 star cells harboring both a pET31b plasmid encoding RNA-based biosensor and a pCOLA plasmid encoding cyclic-di-nucleotide synthetase. Cells were grown aerobically to an OD_{600} ~ 0.3 - 0.5, then induced with 1 mM IPTG at 37 °C for 4 hrs. Cell density was measured by OD_{600}, and diluted in PBS media containing 100 μM DFHBI-1T to a concentration that gives a flow cytometer analysis rate of around 1000 - 2000 events per second. Cellular fluorescence was measured for 30,000 cells using an Attune NxT Acoustic Focusing Cytometer (Life Technologies).

Determination of 2′, 3′-cGAMP concentration in *E. coli* cells overexpressing cGAS

From the linear regression of the standard curve, shown in Figure S3, fitting the standard curve to equation $Y = mX + C$ gave $Y = 2.49X - 7.46$ with an R^2 value of 0.99.

The dry weight of the cGAS expressing cell pallet was 0.75 g. This was lysed, extracted and concentrated to give 250 µL cell extract, and 20 µL of the cell extract was loaded in LC-MS.

Thus, the concentration of 2′,3′-cGAMP in the 20 µL measurement solution was calculated to be:

$$c\ (cGAMP) = \frac{Y - C}{m} = \frac{3372 + 7.46}{2.49 \times 1000}\ mM = 1.36\ mM$$

The amount of 2′,3′-cGAMP in the 250 µL cell extract was:

$$n(cGAMP) = c(cGAMP) \times volume = 1.36\ mM \times 250\ \mu L = 0.34\ \mu mol$$

The dry weight of single E. coli cell is 10^{-12} g, which gives:

$$number\ of\ cells = \frac{cell\ pallet\ weight}{dry\ weight\ of\ single\ cell} = \frac{0.75}{10^{-12}} \approx 0.75 \times 10^{12}$$

The amount of 2,3-cGAMP per cell was determined to be:

$$n(cGAMP\ per\ cell) = \frac{n(cGAMP)}{number\ of\ cells} = \frac{0.34\ \mu mol}{0.75 \times 10^{12}} \approx 0.45 \times 10^{-18}\ \text{mol} = 0.45\ \text{attomol}$$

The volume of *E. coli* cell is 10^{-15} L. The concentration of 2′,3′-cGAMP in cGAS expressing *E. coli* cells was determined as:

$$[cGAMP\ per\ cell] = \frac{n(cGAMP\ per\ cell)}{cell\ volume} = \frac{0.45 \times 10^{-18}\ mol}{10^{-15}\ L} \approx 0.45 \times 10^{-3}\ \text{M} = 0.45\ \text{mM}$$

Determination of 2′, 3′-cGAMP concentration in L929 and HEK293T cell extracts

From the linear regression of the standard curve, shown in Figure 4E, the standard curve fit the equation $Y = mX + C$ gave $1/\text{m} = 1.67 * 10^{-5}\ \mu M$ and $C = 150517 \pm 22135$ with an R^2 value of 0.98.

For measuring the average amount of 2′,3′-cGAMP in each dsDNA-stimulated cell, 6×10^6 DNA-stimulated cells were lysed, extracted and concentrated to give 20 µL cell extract, and 2 µL of the cell extract was added to a solution with final volume of 25 µL for fluorescence measurement. The fluorescence of this solution was measured to be 239874 (figure 4E, average of two independent biological replicates).

Thus, the concentration of 2′,3′-cGAMP in the 25 µL measurement solution was calculated to be:

$$c\ (cGAMP) = \frac{Y - C}{m} = (239874 - 150517) \times (1.67 \times 10^{-5})\ \mu M = 1.5\ \mu M$$

Then, the amount of 2′,3′-cGAMP in the 2 µL cell extract was:

$$n(cGAMP) = c(cGAMP) \times volume = 1.5\ \mu M \times 25\ \mu L = 37\ \text{pmol}$$

Lastly, the amount of 2′,3′-cGAMP per cell was determined as:

$$n(cGAMP\ per\ cell) = \frac{n(cGAMP)}{number\ of\ cells} = \frac{37\ pmol \times 10}{6 \times 10^6} \approx 6 \times 10^{-17}\ \text{mol} = 60\ \text{attomol}$$

$$n(cGAMP\ per\ cell) \approx 6 \times 10^{-17}\ \text{mol} \times \frac{6.022 \times 10^{23}\ molecules}{mol} = 3.6 \times 10^7\ molecules$$

In conclusion, DNA stimulation by transfection resulted in 60 attomoles of 2′, 3′-cGAMP produced on average per L929 cell, or 36 million molecules of 2′, 3′-cGAMP per cell.

Very recently, an LC-MS/MS method has been developed for quantitation of 2′, 3′-cGAMP (Paijo et al., 2016). According to Figure 3 in this research article (Paijo et al., 2016), the amount of 2′, 3′-cGAMP produced upon HCMV virus infection was measured in the range of 1 to 3 fmol/10^4 cells.

$$n(cGAMP\ per\ cell) = \frac{n(cGAMP)}{number\ of\ cells} = \frac{1\ fmol}{10^4} = 1 \times 10^{-19}\ \text{mol} = 0.1\ \text{attomol}$$

$$n(cGAMP\ per\ cell) = 1 \times 10^{-19}\ \text{mol} \times \frac{6.022 \times 10^{23}\ molecules}{mol} \approx 6 \times 10^4\ molecules$$

The current lower limit of detection of our fluorescent biosensor is ~1 µM or 40 attomoles per cell. Thus, improving biosensor sensitivity by 133-($\frac{40\ attomoles}{0.3\ attomoles} = 133$) to 400-fold ($\frac{40\ attomoles}{0.1\ attomoles} = 400$) would provide a high-throughput method to analyze viral-induced 2′, 3′-cGAMP levels.

Supplemental References

Folcher, M., Oesterle, S., Zwicky, K., Thekkottil, T., Heymoz, J., Hohmann, M., Christen, M., Daoud El-Baba, M., Buchmann, P., and Fussenegger, M. (2014). Mind-controlled transgene expression by a wireless-powered optogenetic designer cell implant. Nat Commun *5*, 5392.

Hallberg, Z.F., Wang, X.C., Wright, T.A., Nan, B., Ad, O., Yeo, J., and Hammond, M.C. (2016). Hybrid promiscuous (Hypr) GGDEF enzymes produce cyclic AMP-GMP (3', 3'-cGAMP). Proc Natl Acad Sci U S A *113*, 1790-1795.

Kellenberger, C.A., Chen, C., Whiteley, A.T., Portnoy, D.A., and Hammond, M.C. (2015a). RNA-Based Fluorescent Biosensors for Live Cell Imaging of Second Messenger Cyclic di-AMP. J Am Chem Soc *137*, 6432-6435.

Kellenberger, C.A., Hallberg, Z.F., and Hammond, M.C. (2015b). Live Cell Imaging Using Riboswitch-Spinach tRNA Fusions as Metabolite-Sensing Fluorescent Biosensors. Methods Mol Biol *1316*, 87-103.

Kellenberger, C.A., Wilson, S.C., Hickey, S.F., Gonzalez, T.L., Su, Y., Hallberg, Z.F., Brewer, T.F., Iavarone, A.T., Carlson, H.K., Hsieh, Y.F., *et al.* (2015c). GEMM-I riboswitches from Geobacter sense the bacterial second messenger cyclic AMP-GMP. Proc Natl Acad Sci U S A *112*, 5383-5388.

Kellenberger, C.A., Wilson, S.C., Sales-Lee, J., and Hammond, M.C. (2013). RNA-based fluorescent biosensors for live cell imaging of second messengers cyclic di-GMP and cyclic AMP-GMP. J Am Chem Soc *135*, 4906-4909.

Paijo, J., Doring, M., Spanier, J., Grabski, E., Nooruzzaman, M., Schmidt, T., Witte, G., Messerle, M., Hornung, V., Kaever, V., *et al.* (2016). cGAS Senses Human Cytomegalovirus and Induces Type I Interferon Responses in Human Monocyte-Derived Cells. PLoS Pathog *12*, e1005546.

Ponchon, L., and Dardel, F. (2007). Recombinant RNA technology: the tRNA scaffold. Nat Methods *4*, 571-576.

Song, W., Strack, R.L., Svensen, N., and Jaffrey, S.R. (2014). Plug-and-play fluorophores extend the spectral properties of Spinach. J Am Chem Soc *136*, 1198-1201.

Spangler, C., Bohm, A., Jenal, U., Seifert, R., and Kaever, V. (2010). A liquid chromatography-coupled tandem mass spectrometry method for quantitation of cyclic di-guanosine monophosphate. J Microbiol Methods *81*, 226-231.

Su, Y., Hickey, S.F., Keyser, S.G., and Hammond, M.C. (2016). In Vitro and In Vivo Enzyme Activity Screening via RNA-Based Fluorescent Biosensors for S-Adenosyl-l-homocysteine (SAH). J Am Chem Soc *138*, 7040-7047.

Weber, H., Pesavento, C., Possling, A., Tischendorf, G., and Hengge, R. (2006). Cyclic-di-GMP-mediated signalling within the sigma network of Escherichia coli. Mol Microbiol *62*, 1014-1034.